Monthly Notices
of the
ROYAL ASTRONOMICAL SOCIETY

Mon. Not. R. Astron. Soc. **416,** 1654–1679 (2011) doi:10.1111/j.1365-2966.2011.19113.x

The ATLAS^{3D} project – VI. Simulations of binary galaxy mergers and the link with fast rotators, slow rotators and kinematically distinct cores

Maxime Bois,[1,2]★ Eric Emsellem,[1,2] Frédéric Bournaud,[3] Katherine Alatalo,[4] Leo Blitz,[4] Martin Bureau,[5] Michele Cappellari,[5] Roger L. Davies,[5] Timothy A. Davis,[5] P. T. de Zeeuw,[2,6] Pierre-Alain Duc,[3] Sadegh Khochfar,[7] Davor Krajnović,[2] Harald Kuntschner,[8] Pierre-Yves Lablanche,[1,2] Richard M. McDermid,[9] Raffaella Morganti,[10,11] Thorsten Naab,[12] Tom Oosterloo,[10,11] Marc Sarzi,[13] Nicholas Scott,[5] Paolo Serra,[10] Anne-Marie Weijmans[14]† and Lisa M. Young[15]

[1]*Université Lyon 1, Observatoire de Lyon, Centre de Recherche Astrophysique de Lyon and Ecole Normale Supérieure de Lyon, 9 avenue Charles André, F-69230 Saint-Genis Laval, France*
[2]*European Southern Observatory, Karl-Schwarzschild-Str. 2, 85748 Garching, Germany*
[3]*Laboratoire AIM Paris-Saclay, CEA/IRFU/SAp CNRS Université Paris Diderot, 91191 Gif-sur-Yvette Cedex, France*
[4]*Department of Astronomy, Campbell Hall, University of California, Berkeley, CA 94720, USA*
[5]*Sub-department of Astrophysics, University of Oxford, Denys Wilkinson Building, Keble Road, Oxford OX1 3RH*
[6]*Sterrewacht Leiden, Leiden University, Postbus 9513, 2300 RA Leiden, the Netherlands*
[7]*Max-Planck-Institut für extraterrestrische Physik, PO Box 1312, D-85478 Garching, Germany*
[8]*Space Telescope European Coordinating Facility, European Southern Observatory, Karl-Schwarzschild-Str. 2, 85748 Garching, Germany*
[9]*Gemini Observatory, Northern Operations Centre, 670 N. A'ohoku Place, Hilo, HI 96720, USA*
[10]*Netherlands Institute for Radio Astronomy (ASTRON), Postbus 2, 7990 AA Dwingeloo, the Netherlands*
[11]*Kapteyn Astronomical Institute, University of Groningen, Postbus 800, 9700 AV Groningen, the Netherlands*
[12]*Max-Planck-Institut für Astrophysik, Karl-Schwarzschild-Str. 1, 85741 Garching, Germany*
[13]*Centre for Astrophysics Research, University of Hertfordshire, Hatfield, Herts AL1 9AB*
[14]*Dunlap Institute for Astronomy & Astrophysics, University of Toronto, 50 St George Street, Toronto, ON M5S 3H4, Canada*
[15]*Physics Department, New Mexico Institute of Mining and Technology, Socorro, NM 87801, USA*

Accepted 2011 May 20. Received 2011 May 20; in original form 2010 November 24

ABSTRACT

We study the formation of early-type galaxies (ETGs) through mergers with a sample of 70 high-resolution (softening length $<$60 pc and 12×10^6 particles) numerical simulations of binary mergers of disc galaxies (with 10 per cent of gas) and 16 simulations of ETG remergers. These simulations, designed to accompany observations and models conducted within the ATLAS^{3D} project, encompass various mass ratios (from 1:1 to 6:1), initial conditions and orbital parameters. The progenitor disc galaxies are spiral-like with bulge-to-disc ratios typical of Sb and Sc galaxies and high central baryonic angular momentum. We find that binary mergers of disc galaxies with mass ratios of 3:1 and 6:1 are nearly always classified as fast rotators according to the ATLAS^{3D} criterion (based on the λ_R parameter – ATLAS^{3D} Paper III): they preserve the structure of the input fast rotating spiral progenitors. They have intrinsic ellipticities larger than 0.5, cover intrinsic λ_R values between 0.2 and 0.6, within the range of observed fast rotators. The distribution of the observed fastest rotators does in fact coincide with the distribution of our disc progenitors. Major disc mergers (mass ratios of 2:1 and 1:1) lead to both fast and slow rotators. Most of the fast rotators produced in major

★E-mail: maxime.bois@obspm.fr
†Dunlap Fellow.

mergers have intermediate flattening, with ellipticities ϵ between 0.4 and 0.6. Most slow rotators formed in these binary disc mergers hold a stellar kinematically distinct core (KDC) in their ∼1–3 central kiloparsec: these KDCs are built from the stellar components of the progenitors. However, these remnants are still very flat with ϵ often larger than 0.45 and sometimes as high as 0.65. Besides a handful of specific observed systems – the counter-rotating discs (2σ galaxies, ATLAS^{3D} Paper II) – these therefore cannot reproduce the observed population of slow rotators in the nearby Universe. This sample of simulations supports the notion of slow and fast rotators: these two families of ETGs present distinct characteristics in term of their angular momentum content (at all radii) and intrinsic properties – the slow rotators are not simply velocity-scaled down versions of fast rotators. The mass ratio of the progenitors is a fundamental parameter for the formation of slow rotators in these binary mergers, but it also requires a retrograde spin for the earlier-type (Sb) progenitor galaxy with respect to the orbital angular momentum. We also study remergers of these merger remnants: these produce relatively round fast rotators or systems near the threshold for slow rotators. In such cases, the orbital angular momentum dominates the central region, and these systems no longer exhibit a KDC, as KDCs are destroyed during the remergers and do not re-form in these relatively dry events.

Key words: methods: numerical – galaxies: elliptical and lenticular, cD – galaxies: formation – galaxies: interactions – galaxies: kinematics and dynamics.

1 INTRODUCTION

Numerical simulations, intensively used for more than two decades, have clearly shown that the global characteristics of the remnants of binary merger between two equal-mass spiral galaxies, called major mergers, resemble those of early-type galaxies (i.e. ellipticals and lenticulars), hereafter ETGs (Toomre & Toomre 1972; Hernquist & Barnes 1991; Barnes 1992; Mihos et al. 1995; Springel 2000; Naab & Burkert 2003; Bournaud, Jog & Combes 2005). Remnants with properties similar to ETGs can also be recovered via multiple minor mergers with the total accreted mass being at least half of the initial mass of the main progenitor (Weil & Hernquist 1994, 1996; Bournaud, Jog & Combes 2007). This picture of the formation of ETGs via accretion and merging of stellar bodies would fit well within the frame of the hierarchical assembly of galaxies provided by Λ cold dark matter (ΛCDM) cosmology.

Owing to large statistical samples, modern work tends to quantify in detail the properties of major and minor merger remnants, together with thorough comparisons with observed properties of ETGs (Naab & Burkert 2003; Bournaud, Combes & Jog 2004; Bournaud, Jog & Combes 2005; Naab, Jesseit & Burkert 2006a; Cox et al. 2006a, 2008; Rothberg & Joseph 2006; Di Matteo et al. 2007; Burkert et al. 2008; Jesseit et al. 2009; Hoffman et al. 2010; Chilingarian et al. 2010). It is, however, still difficult to build large samples of simulations with sufficiently high numerical resolution. Many studies have indeed shown that the resolution affects the properties of the simulated objects, either in cosmological simulations (Naab et al. 2007; Navarro et al. 2010) or on simulations of star formation in mergers (Cox et al. 2006b; Hopkins et al. 2008; Di Matteo et al. 2008; Wuyts et al. 2010). Bois et al. (2010) claimed that a high-enough resolution is required to resolve properly the fluctuations of the gravitational potential during the merger, i.e. violent relaxation, which can significantly impact the morphology and kinematics of merger remnants.

In this paper, we further examine the role of the initial conditions (impact parameter, incoming velocities, inclination and spins of the progenitors) on the global characteristics of the remnants of binary galaxy mergers. We then propose to study the morphology and the kinematics of binary galaxy merger remnants simulated with a high numerical resolution. With that purpose in mind, we build two-dimensional (2D) momentum (intensity, velocity and velocity dispersion) maps of the merger remnants and analyse their apparent properties, directly linked with their orbital structures (Jesseit, Naab & Burkert 2005). Using 2D maps enables us to compare our merger remnants directly with modern spectroscopic observations of resolved local galaxies: the emergence of integral field spectrographs, such as the SAURON spectrograph (Bacon et al. 2001), allowed the mapping of local ETGs up to about one effective radius. Numerical simulations of binary mergers of disc galaxies or binary remergers are not necessarily representative of observed ETG (Rothberg & Joseph 2006; Burkert et al. 2008) but they are a powerful tool to constrain the formation mechanisms of different features observed in 2D maps of local galaxies like e.g. the formation of kinematically distinct cores (KDC) (e.g. Hernquist & Barnes 1991; Jesseit et al. 2009; Bois et al. 2010; Hoffman et al. 2010), the presence of gaseous discs (e.g. Hopkins et al. 2009; Martig et al. 2009), the relation between nuclear black holes and the dynamics of the stars (e.g. Springel, Di Matteo & Hernquist 2005; Johansson, Naab & Burkert 2009), the formation of plumes, tails, stellar clusters at large radii or giant gas rings (Feldmann, Mayer & Carollo 2008; Bournaud, Duc & Emsellem 2008; Michel-Dansac et al. 2010).

The SAURON survey (de Zeeuw et al. 2002) has introduced a new view of ETGs, classifying them in two families – the fast and the slow rotators – according not only to their morphology, but also to their kinematics (Cappellari et al. 2007; Emsellem et al. 2007, hereafter E+07; see also Section 2.2.3). These two classes are intrinsically different and seem to correspond to different populations of galaxies: while the fast rotators present regular rotation patterns aligned with the photometry, the slow rotators have low angular momentum and show misalignments between the photometry and the velocity axes. Furthermore, slow rotators often exhibit KDCs, usually defined as a central stellar component with a rotation axis distinct from the outer stellar body (see e.g. Krajnović et al. 2008). KDCs have been claimed to be a signature of a past interaction (e.g. Franx & Illingworth 1988; Jedrzejewski & Schechter 1988; de Zeeuw & Franx 1991; Scorza & Bender 1995; Davies et al. 2001).

To further constrain the formation scenarios for these two classes, an ambitious programme – ATLAS^{3D} – is being conducted, combining a multi-wavelength observational survey of a complete volume-limited sample of ETGs with various numerical simulation and modelling efforts. The ATLAS^{3D} project[1] (Cappellari et al. 2011, hereafter Paper I) aims to quantify the distribution and kinematics of the stellar and gaseous components of a statistically significant sample of ETGs to relate their detailed properties to their mass assembly, star formation history and evolution. Krajnović et al. (2011, hereafter Paper II) introduced new subclasses within the slow rotator class: non-rotators which do not show any apparent sign of rotation, galaxies with a KDC when there is an abrupt change in the radial profile of the kinematical position angle ($>30^\circ$), galaxies with non-regular velocity pattern but with no noticeable kinematic feature and the 2σ galaxies characterized by two off-centred symmetric dispersion peaks along the major-axis. These so-called 2σ galaxies are generally thought to have two stellar counter-rotating components (i.e. a KDC at 180° away from the outer body) (see also Jesseit et al. 2007, for 2D-map examples of these counter-rotating components in simulations).

In the context of the ATLAS^{3D} project, an extensive set of numerical simulations is being conducted to support the survey: cosmological simulations, semi-analytic modelling and idealized binary galaxy mergers. In the present study, we have simulated a substantial sample ($\sim$90) of binary mergers of disc galaxies and binary galaxy remergers at an unprecedented resolution, sufficient to properly follow the merging process and the resulting galaxy remnant (Bois et al. 2010). We aim to constrain the formation of the slow and fast rotators revealed by the SAURON survey. For this purpose, we look at the morphology and the kinematics of the binary merger and remerger remnants and link the initial conditions of the mergers to the formation of the fast and slow rotators as well as the formation of the KDCs. In Section 2, we present the initial progenitor galaxies, which are spirals of Hubble-type Sb and Sc, and the different initial conditions of merging. We present in Section 3 the global properties of the merger remnants and the impact of the initial conditions: we thus show that the mass ratio, the angular momentum content and the Hubble type of the progenitors play an important role in the formation of the slow and fast rotators and the KDCs. In Section 4, we analyse the remnants of galaxy remergers; these remnants are all classified as fast rotators or near the threshold for slow rotators and do not show any trace of a KDC. The formation mechanism of the KDCs via binary mergers of disc galaxies is presented in Section 5. We then discuss our results and compare it with previous studies (Section 6) and with the observations of the 260 ETGs of the ATLAS^{3D} survey (Section 7). We then conclude and sum-up all our results in Section 8.

2 SIMULATIONS AND ANALYSIS

2.1 Method

2.1.1 Code

We use the particle-mesh code described in Bournaud et al. (2008), Bois et al. (2010) and references therein. This code uses a Cartesian grid on which the particles are meshed with a 'Cloud-In-Cell' interpolation. The gravitational potential is computed with an FFT-based Poisson solver and particle motions are integrated with a time-step of 0.5 Myr. All simulations in this paper were performed with a softening length (i.e. spatial resolution) of 58 pc.

Interstellar gas dynamics are modelled with the sticky-particle scheme with elasticity parameters $\beta_t = \beta_r = 0.6$. This scheme neglects the thermal pressure of the gas, assuming it is dominated by its turbulent pressure, which is the case for the bulk of the gas mass in the star-forming interstellar medium (Elmegreen & Scalo 2004; Burkert 2006). The velocity dispersion of the gas particles models the turbulent speed, and their collisions model the turbulent pressure. The collisions are inelastic to ensure that the modelled turbulence dissipates in about a vertical crossing time in discs (Mac Low 1999).

Star formation is modelled with a local Schmidt law (Schmidt 1959; Kennicutt 1998): the star formation rate in each resolution element is proportional to the gas density to the exponent 1.5. Energy feedback from supernovae is accounted for with the kinetic scheme initially proposed by Mihos & Hernquist (1994). Each stellar particle formed has a number of supernovae computed from the fraction of stars above 8 $M_\odot$ in a Miller–Scalo initial mass function. A fraction ϵ of the typical 10^{51} erg energy of each supernova is released in the form of radial velocity kicks applied to gas particles within the closest cells. We use $\epsilon = 2 \times 10^{-4}$, as Mihos & Hernquist (1994) suggested that realistic values lie around 10^{-4} and less than 10^{-3}. Simulations with parsec-scale resolution have to use much higher values for the ϵ parameter (e.g. Bournaud et al. 2010): the low value of the ϵ parameter used here reflects the fact that a large fraction of the released energy is radiated away (through dissipation and gas cooling processes) before spreading on scales of 50–100 pc (i.e. the resolution of our present models). Larger values of ϵ would thicken the gas discs of isolated spirals to unacceptable proportions (Mihos & Hernquist 1994; Elmegreen, Bournaud & Elmegreen 2008).

2.1.2 Set-up for initial parameters

We have simulated binary mergers of discs galaxies (i.e. 'spiral–spiral' mergers) with mass ratios of 1:1, 2:1, 3:1 and 6:1. The main parameters are summarized in Table 1 for the progenitor galaxies and Table 2 for the orbital parameters. Table 3 summarizes the parameters used for remergers using the result of a first merger simulation as an input for a new merger simulation (i.e. 'spiral-ETG' or 'ETG-ETG' mergers).

Initial progenitor galaxies. Our main sample consists of binary mergers of disc galaxies, i.e. 'spiral–spiral' mergers. The first progenitor, which is defined as the most massive for unequal-mass mergers, has a baryonic mass of 1.3×10^{11} $M_\odot$. The bulge fraction is $B/T = 0.20$ and the gas fraction in the disc is usually 10 per cent (33 per cent in some m21 simulations). The initial disc has a Toomre profile[2] with a scalelength of 4 kpc, consistent with observations of nearby disc galaxies (Fathi et al. 2009), truncated at 10 kpc. The gas has a scalelength of 8 kpc and a truncation radius of 20 kpc. The bulge has a Hernquist (1990) profile with a scalelength of 700 pc. The dark matter halo is modelled with a Burkert profile (Burkert 1995) with a 7 kpc scalelength and a truncation radius of 70 kpc, inside which the dark matter mass is 3×10^{11} $M_\odot$. This initial galaxy is representative for an Sb spiral galaxy, given its bulge fraction in particular (Graham & Worley 2008), and is denoted as the *Sb* spiral progenitor throughout the paper.

[1] http://purl.org/atlas3d

[2] The profile rapidly evolves into a quasi-exponential profile with a slightly smaller exponential scalelength.

Table 1. Main physical parameters used to model the initial progenitor galaxies in our merger models. (1) Spiral Hubble type, (2) $M_{\rm stars}$ in the bulge/total $M_{\rm stars}$, (3) fraction of the baryonic mass in gas, (4) Baryonic mass in unit of $1.3 \times 10^{11}\,{\rm M}_{\odot}$ and (5) total number of particles (stars, gas and dark matter).

Name	Prog 1$^{(1)}$	$B/T^{(2)}$	$f_{\rm gas}^{(3)}$ (per cent)	$m_B^{(4)}$	$N_{\rm part}^{(5)}$	Prog 2$^{(1)}$	$B/T^{(2)}$	$f_{\rm gas}^{(2)}$ (per cent)	$m_B^{(3)}$	$N_{\rm part}^{(5)}$
m11	Sb	0.2	10	1	6×10^6	Sc	0.12	10	1	6×10^6
m21g10	Sb	0.2	10	1	6×10^6	Sc	0.12	10	0.5	3×10^6
m21g33	Sb	0.2	33	1	6×10^6	Sc	0.12	33	0.5	3×10^6
m31	Sb	0.2	10	1	6×10^6	Sc	0.12	10	0.33	2×10^6
m61	Sb	0.2	10	1	6×10^6	Sc	0.12	15	0.17	1×10^6

Table 2. The different initial conditions for the mergers. (1) The relative incoming velocity V_∞ (in km s^{-1}) of the Sc companion computed at infinite distance. (2) Inclination i (in degrees) for each galaxy with respect to the orbital plane. (3) Impact parameter R at infinite distance (in kpc).

Name	V_∞ $^{(1)}$	i $^{(2)}$	R $^{(3)}$
0	120	45	60
im	120	25	60
ip	120	75	60
Rm	120	45	35
Vm	70	45	60
Vp	200	45	60

Table 3. Details of the characteristics of the remergers: (1) Spin of the progenitors with respect to the orbital angular momentum, (2) galaxy remnants of binary merger of spirals as progenitors for the remerger and (3) slow/fast classification from Section 3.1.

Name	Orbit$^{(1)}$	Progenitors$^{(2)}$	Prog type$^{(3)}$
rem2x11	dd	rd0–rr0	Slow–slow
rem2x11	dr	rrim–ddip	Slow–fast
rem2x11	rd	rrVp–ddVm	Slow–fast
rem2x11	rr	rd0–dd0	Slow–fast
rem2x21g10	dd	rd0–rr0	Slow–slow
rem2x21g10	dr	rrim–ddip	Slow–fast
rem2x21g10	rd	rrVp–ddVm	Slow–fast
rem2x21g10	rr	rd0–dd0	Slow–fast
rem2x21g33	dd	rd0–rr0	Slow–slow
rem2x21g33	dr	rrim–ddip	Slow–fast
rem2x21g33	rd	rrVp–ddVm	Slow–fast
rem2x21g33	rr	rd0–dd0	Slow–fast
rem21g10+S	dd	rr0–S	Slow–fast
rem21g10+S	dr	rdim–S	Slow–fast
rem21g10+S	rd	rdVp–S	Slow–fast
rem21g10+S	rr	dd0–S	Fast–fast

The other progenitor, which has the lower mass in unequal mass mergers, has its total mass determined by the mass ratio. Apart from the bulge which was reduced to $B/T = 0.12$, all components have their mass scaled by a factor equal to the mass ratio, and all sizes and scalelengths scaled by the square root of the mass ratio, thus keeping the central density of their discs constant. The gas fraction is 10 per cent, except for the lower mass companions used in 6:1 mergers where a gas fraction of 15 per cent is used. The main difference with the first progenitor is thus the lower bulge fraction. Following Graham & Worley (2008) this galaxy is classified as an Sbc spiral; but for convenience, this progenitor galaxy will be denoted as the *Sc* spiral progenitor.

The Sb spiral is modelled with 2×10^6 particles for each component (stars, gas and dark matter). The Sc spiral is modelled with a number of particles scaled by the mass ratio. Equal-mass mergers thus use a total of 12 million particles.

The progenitors are initialized as perfectly axisymmetric disc galaxies. Such galaxies will unavoidably develop substructures such as spiral arms, bars, etc. We need to avoid this spontaneous, intrinsic evolution from taking place during the merger, otherwise the effects of the merger itself cannot be disentangled. We also need to avoid the artificial consumption of gas that could result from applying the Schmidt law during the transition from an axisymmetric gas disc to a spiral disc. To this aim, each progenitor galaxy was evolved in isolation and without star formation for about two rotations of the outer stellar disc, so that a reasonable steady state in its structure and gas density distribution is reached. At this point, we remark that the Sb progenitor is more concentrated and dynamically stable than the Sc galaxy. The merger simulation is then started, with star formation and feedback, using these pre-evolved progenitors (see Martig & Bournaud 2008 for further discussion on this technique).

The initial properties of our pre-merger spiral galaxies, after their initial relaxation in isolation, are shown in Fig. 1. We in particular compare the isophotal ellipticity ϵ to their angular momentum tracer $\lambda_{\rm R}$ at the effective radius $R_{\rm e}$ for 200 different projections (see Sections 2.2.1 and 2.2.3 for details on the ϵ and $\lambda_{\rm R}$ parameters and on the projection effects). Small differences between the progenitors arose during the initial relaxation as galaxies with different sizes and bulge fractions behave somewhat differently in isolation; these properties are essentially stabilized (on time-scales of a few 10^8 yr) when the merger simulations are started.

Merger orbits. The different orbits used for the merger simulation are described in Table 2. They are all parabolic or hyperbolic, with an initial total energy $E > 0$ or $E \simeq 0$, corresponding to initially unbound galaxy pairs. Such orbits are representative of the most common mergers in ΛCDM cosmology (Khochfar & Burkert 2006).

The fiducial orbit '0' has a velocity at infinite distance of $V_\infty = 120\,{\rm km\,s^{-1}}$, an inclination $i = 45^\circ$ for each galaxy with respect to the orbital plane and an impact parameter (i.e. the perpendicular distance between the two velocity vectors of the progenitors at the beginning of the simulation) of $R = 60\,{\rm kpc}$. The six other orbits correspond to one of the three parameters V, R, i being changed compared to the fiducial values, one at a time. The nomenclature denotes the parameter varied and whether it is increased (p: plus) or decreased (m: minus), as detailed in Table 2. We have then a total of 70 simulations of galaxy mergers.

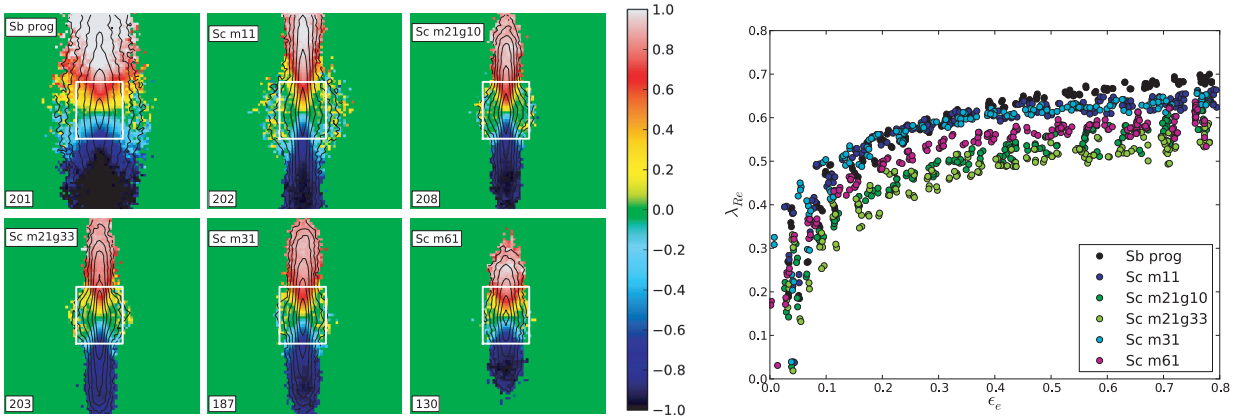

Figure 1. Left: projected stellar velocity maps for the Sb progenitor and the different mass ratio Sc companions; the black contours represent the iso-magnitude contours; they are equally spaced in magnitude and are the same for all progenitors. Each subpanel is labelled with the name of the progenitor and with the maximum velocity $V_{\rm max}$, the colour bar goes from $-V_{\rm max}$ to $+V_{\rm max}$. The field of view is 15 × 15 kpc^2 (15 kpc $\simeq 6R_{\rm e}$). The white rectangle indicates a typical field covered by the instrument SAURON and corresponds to a field of 41 × 33 arcsec^2 for a galaxy at a distance of 20 Mpc; its orientation follows the photometric position angle taken at $3R_{\rm e}$. Right: $\lambda_{\rm R}$–ϵ diagram for the progenitors of binary mergers. The Sb progenitor (black points) is the same in all simulations, the other colours correspond to the Sc companion at different mass ratios (m11 in blue, m21g10 in green, m21g33 in light green, m31 in cyan and m61 in magenta). All projections (200 per remnant) are plotted.

In addition to the three listed parameters, we identify the spin of the progenitors which can be either direct (prograde) *d* or retrograde *r* with respect to the orbital angular momentum. The first letter refers to the spin of the first progenitor (Sb) and the second letter to the Sc companion.

Our nomenclature also indicates the type (mass ratio) of the modelled merger, as defined in Table 1. For instance, the simulation labelled *m31rdVm* refers to a 3:1 merger with a retrograde orientation for the main Sb progenitor and a direct orientation for the Sc companion on an orbit with lowered initial velocity.

The chosen orbits do not cover all the parameter space of initial conditions: the goal of this paper is to understand the formation of slow and fast rotators, and not to build a full library of binary merger remnants.

2.2 Analysis

We analysed all merger remnants about 600-800 Myr after the central coalescence. The central body of the ETG-like systems formed in the mergers is thus relaxed within several effective radii when the analysis is performed, even if tidal debris is present at larger radii. We checked in several cases that the measured morphological and kinematical parameters were stabilized by comparing the ellipticity and the $\lambda_{\rm R}$ parameter to earlier snapshots.

2.2.1 Projected velocity moment maps

Intrinsic and apparent properties of the merger remnant, such as the apparent ellipticity, are directly linked with its orbital structure (Jesseit et al. 2005). To probe the intrinsic properties of the relaxed merger remnants in a way that is comparable to observations, we have therefore built velocity moment maps indicating the stellar surface density, stellar velocity field and stellar velocity dispersion for various projections. 2D maps are useful to reveal the wealth of photometric or kinematic structures associated with a galaxy merger remnant, such as young stellar clusters (potentially globular clusters; Bois et al. 2010), kinematic misalignments (Bendo & Barnes 2000; Jesseit et al. 2007; Krajnović et al. 2008), and are also used to measure various parameters with definitions finely matching those used for the ATLAS$^{\rm 3D}$ observations (see below).

The intensity and velocity moment maps are built to cover a 20 × 20 kpc^2 field of view around the stellar density peak of each system (figures show the inner 15 × 15 kpc^2 area). This covers at least about four effective radii $R_{\rm e}$ to enclose most of the baryonic mass of ETG, the average effective radius of our merger remnants being 2.3 kpc. Each projection was computed on a 100 × 100 pixel grid, giving an effective resolution consistent with the SAURON data of the ATLAS$^{\rm 3D}$ survey. The maps have been Voronoi binned (Cappellari & Copin 2003) to have a minimum number of 400 particles per bin.

To obtain statistically representative results rather than analysing a particular projection, we have produced velocity moment maps and performed the subsequent analysis for 200 isotropically distributed viewing angles for each merger remnant. The choice of 200 projections ensures a sampling smaller than 10° in any direction, so that intermediate viewing angles would not show significant differences.

2.2.2 The presence of KDCs

The merger remnants analysed in the following sections often exhibit a central stellar component with an apparent rotation axis distinct from the one of the outer parts. In the present study, using the definition given by Krajnović et al. (2008), we have conducted a visual inspection of the velocity maps to detect such central structures and flag them as KDCs. The use of this objective criterion leads to clear signatures of the KDCs which are easily recognizable.

In the 2D velocity maps of the merger remnants presented in Appendix A, we indicate the typical field covered by the instrument SAURON (a field of view typically of 41 × 33 arcsec^2) for a galaxy at a distance of 20 Mpc. We note that a few KDCs in the merger remnants (see Section 3 for the properties of these galaxies and the formation processes of the KDCs) are larger than that typical SAURON field. This obviously depends on the distance of the system, as SAURON would fully cover these KDCs for galaxies at distances larger than e.g., 30 Mpc. In the following sections, we show that the merger remnants with a KDC – even those which are larger than the SAURON field of view – are all classified as slow

rotators and have properties which are distinct from those of the fast rotators.

With numerical simulations, we can easily investigate the stellar kinematics of galaxies at large radii to probe, e.g., large KDCs. It is observationally much more challenging with, e.g., the SAURON field of view being limited to approximately one effective radius for local ETGs. This may lead to (a few) mis-identifications. New promising techniques are emerging which should allow us to explore the faint outer stellar structures of larger samples of ETGs (see e.g. Weijmans et al. 2009; Coccato et al. 2009; Proctor et al. 2009; Murphy, Gebhardt & Adams 2011, or the SAGES project).

2.2.3 Extracted parameters

Our analysis is mainly based on two simple morphological and kinematic parameters, a choice motivated by the fact that these parameters are often used as standards in studies of nearby ETGs (e.g. Jesseit et al. 2009; Bois et al. 2010). The analysis in this paper assumes a constant stellar mass-to-light ratio, which should be a reasonable approximation for relatively old ETGs. Furthermore, our main results will show that the classification of merger remnants into slow and fast rotators, and the presence of KDCs, does not significantly depend on the youngest stellar populations formed during the merger, but rather on how the populations from each progenitor galaxy are distributed with respect to each others.

To quantify the global morphology, we measured the ellipticity $\epsilon = 1 - b/a$, where a and b are the semimajor and minor axes, respectively. To measure a profile of a, b and ϵ as a function of the radius r [and subsequently an $\epsilon(a)$ profile], we selected all pixels encircled by a given isophote and computed the inertia matrices as in e.g. Cappellari et al. (2007). The diagonalization of these matrices provides ϵ and the position angle (PA) of the projected density map at different radii r. We also derive the effective radius R_e from the stellar surface density as the radius encompassing half of the total stellar light (or stellar mass).

To quantify the global kinematics of each system, using the velocity and velocity dispersion maps, we measure the λ_R parameter, which is a robust proxy for the stellar projected angular momentum defined in E+07 :

$$\lambda_R \equiv \frac{\langle R\,|V|\rangle}{\langle R\sqrt{V^2+\sigma^2}\rangle}.$$

We hence compute λ_R profiles for all projections of all merger remnants. This is achieved by selecting all pixels enclosed within the ellipse defined by the position angle and axial ratio of the photometric inertia matrix, mirroring the procedure described in E+07:

$$\lambda_R = \frac{\sum_{i=1}^{N_p} F_i R_i\,|V_i|}{\sum_{i=1}^{N_p} F_i R_i \sqrt{V_i^2+\sigma_i^2}},$$

where F_i is the flux inside the ith pixel inside the ellipse, R_i its distance to the centre, and V_i and σ_i the corresponding mean stellar velocity and velocity dispersion values of the pixel.

In E+07, λ_R was used to reveal two families of ETG, the slow rotators with $\lambda_R \leq 0.1$ and the fast rotators with $\lambda_R > 0.1$ at one effective radius R_e. Jesseit et al. (2009) have simulated binary disc mergers to further investigate the λ_R parameter, and have shown that λ_R is a good indicator of the true angular momentum content in ETGs, as confirmed via the knowledge of the full phase-space distribution in the corresponding remnants. As emphasized in E+07, Cappellari et al. (2007) and Krajnović et al. (2008), fast and slow rotators exhibit qualitatively and quantitatively different stellar kinematic properties. Our following analysis will lend further support to the fact that λ_R can really separate two classes of galaxies and that the distinction of fast and slow rotators does not simply result from an arbitrary λ_R threshold.

The SAURON survey was based on a representative sample of ETGs but biased towards the upper end of the luminosity function. The ATLAS^{3D} survey probes a complete sample of ETGs in the Local volume (Paper I). This led to an improved criterion for the separation between fast and slow rotators with $\lambda_R = 0.31 \cdot \sqrt{\epsilon}$ at one effective radius R_e (see Emsellem et al. 2011, hereafter Paper III).

The main analysis performed in this paper is then based on the λ_R–ϵ diagram plotted at $1R_e$. When the merger remnant presents a strong bar and/or strong spiral arms, the ellipticity is computed at $3R_e$ to better account for the outer ellipticity and avoid being contaminated by the flattening of the bar (the difference being significant only for a small fraction of the projections), and λ_R always being computed at R_e. This is the same procedure applied to the real ATLAS^{3D} galaxies in Paper III and makes our results directly comparable to the observations.

The right-hand panel of Fig. 1 shows the values of ϵ and λ_R for the 200 projections of the various disc progenitors. A few generic statements, valid for any of our spiral progenitors as well as for our fast rotator merger remnants (see Section 3), can be made (see also Jesseit et al. 2009):

(i) the edge-on view (high ϵ) of the progenitors has, as expected, the highest λ_R value.

(ii) as the galaxy is inclined (lower ϵ) the value of λ_R slightly decreases.

(iii) as the viewing angle gets nearly face-on, the value of λ_R drops abruptly, reaching $\lambda_R \simeq 0$ for $\epsilon \simeq 0$ as expected.

3 BINARY MERGERS OF DISC GALAXIES: SLOW AND FAST ROTATORS

This section is devoted to the analysis of the remnants of binary mergers of disc galaxies, which in our sample are Sb+Sc mergers with various orbits and mass ratios. We study under which conditions slow and fast rotators are formed, according to the criterion defined in Section 2.2.3. We will provide a more direct comparison between the properties of the simulated slow and fast rotators with the galaxies of the ATLAS^{3D} sample of nearby ETGs in Section 7. We also study which of the merger remnants harbour a KDC, and study the influence of the internal and orbital parameters of the merger in determining such properties.

3.1 General results: populations of slow and fast rotators

The λ_R–ϵ diagram is a useful tool to quantify the global properties of ETGs: it relates the angular momentum and flattening at one effective radius R_e, and disentangles fast and slow rotators. Fig. 2 shows this diagram for our complete sample of 70 binary disc merger simulations, including the 200 independent projections analysed for each relaxed merger remnant. The threshold defined by $\lambda_R = 0.31 \cdot \sqrt{\epsilon}$ separating slow and fast rotators as suggested by the ATLAS^{3D} observations is shown (Paper III). Each set of projections for a given simulation spans a range of λ_R–ϵ values: this is shown in Fig. 2 and individual examples are presented in Fig. 3 as well as in Fig. 4 for various mass ratios. Fig. 3 also shows examples of velocity moment maps for several fast and slow rotators formed in 1:1, 2:1 and 3:1 mergers.

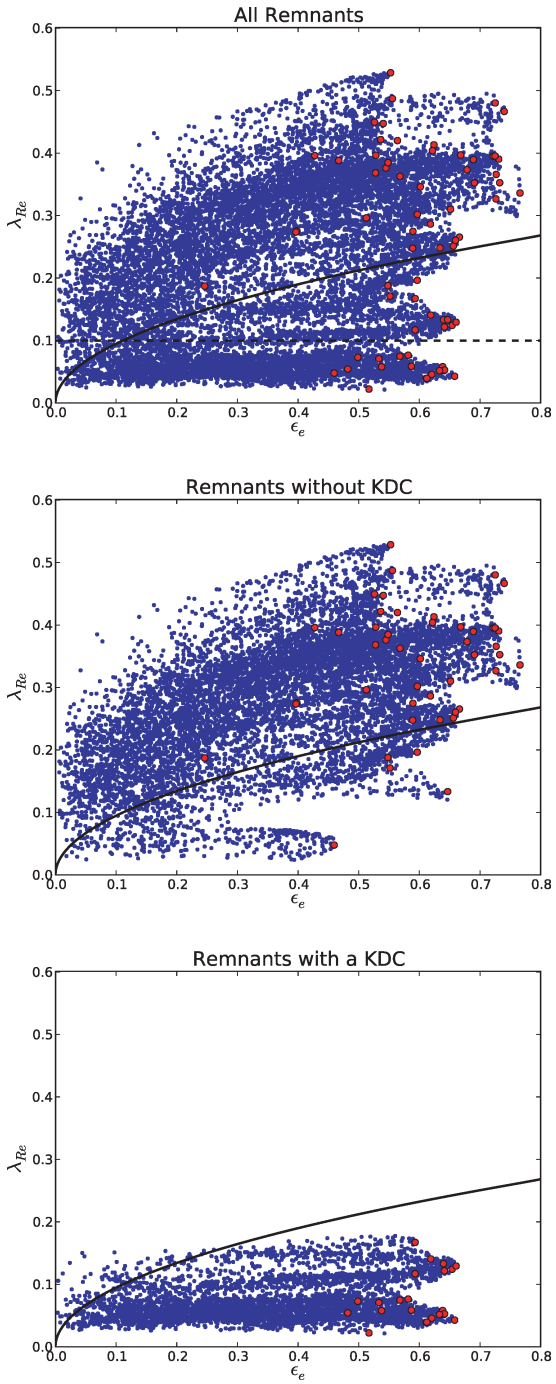

Figure 2. Top: λ_R–ϵ diagram for all simulations of binary mergers of disc galaxies. All projections (200 per remnant) are plotted in blue, the red symbols corresponding to the maximum ellipticity (i.e. edge-on view) of a remnant. The limits defining the slow/fast categories from ATLAS^{3D} (solid) and from SAURON (dashed, only for the top panel) are plotted in black. Middle: same diagram for the simulations which do not present a KDC in their velocity fields. Bottom: same diagram for the simulations which present a KDC in their velocity fields.

The λ_R–ϵ distribution for our entire sample of binary merger remnants is shown in Fig. 2 for galaxies with and without a KDC, respectively. The merger remnants can be seen in Appendix A; the colour code in the different panels presents in black the fast rotators, in red the slow rotators with KDC and in green the slow rotators without KDC. Fig. 2 shows evidence for a tight relation between the presence of a KDC and the slow versus fast rotator classification. All fast rotators presented in Fig. 3 show a clear and regular rotation pattern at all radii, and most slow rotators exhibit KDCs.

We can then sketch the following general results regarding the formation of fast and slow rotators and the presence of a KDC from our sample of binary disc mergers:

(i) We find both fast and slow rotators in our sample of relaxed remnants of binary disc mergers. An *apparent* bimodality is observed in the global λ_R–ϵ distribution of the sample and in the presence of a KDC in the remnants. This could likely result from the specific choices of simulated mass ratios and the limited number of simulated incoming orbits.

(ii) In our sample of merger remnants, fast rotators all have aligned kinematic and photometric axes, while slow rotators frequently exhibit kinematic misalignments (see Section 7.2 and examples in Fig. 3), and obviously weak rotational support. This is similar to what is observed in the ATLAS^{3D} sample (Paper II). This suggests that slow rotators are not velocity-scaled down versions of members of the fast rotator population.

(iii) Slow rotators remain slow for nearly all viewing angles, and fast rotators remain fast. Even nearly face-on projections of fast rotators are rarely classified as 'slow'. This result was already pointed out by Jesseit et al. (2009) while using a constant threshold for λ_R between slow and fast rotators as in E+07. The simulations allow here to further explore various projections of a given merger remnant: they confirm that the combination of the λ_R and ϵ parameters, together with the refined definition for fast and slow rotators recently proposed in Paper III (see Section 2.2), allows a robust classification of ETGs, which is almost independent of the viewing angles.

(iv) Another intrinsic difference between fast and slow rotators is that none of the fast rotators harbours a KDC, while the majority of slow rotators do harbour a clear KDC. Only for a few slow rotators we could not detect a clear KDC (with sufficient rotation amplitude or misalignment angle). This strong trend brings further support to the relevance of the definition of fast and slow rotators as emphasizing two families with different intrinsic properties. With the low noise level and very high velocity resolution of our simulations, we notice that KDCs in slow rotators are visible for the vast majority of projections, but sometimes with rather low-velocity amplitudes which would be hard to detect in observations.

(v) Slow rotators have relatively high edge-on ellipticities (0.45 to 0.65), with the ones for fast rotators being only slightly larger (generally 0.5 to 0.75). The mean ellipticities over random projections show a somewhat more significant though still mild difference, being around 0.35 for slow rotators and 0.45 for fast rotators. The fast rotators with the highest edge-on ellipticities ($\epsilon > 0.7$) are remnants of some of the less violent 3:1–6:1 mergers; those which tend to appear rounder formed with high orbital inclinations. We also note that the majority of fast rotators have a bar, and 6:1 merger remnants often have weak spiral arms associated with the bars.

(vi) The typical λ_R profile of a fast rotator (see Figs A1 to A5 in the Appendix) increases rapidly within 1 to 2 effective radii, and then exhibits a shallower positive slope. As for slow rotators, we observe two general types of λ_R profiles. (1) It can remain constant with a low value within 1.5 or $2R_e$ and then starts to slightly increase outwards or (2) λ_R shows a local maximum around $0.5R_e$, decreasing from there to $\sim 1R_e$, with a subsequent outwards increase: such a λ_R profile is the clear signature of large-scale KDC as mentioned

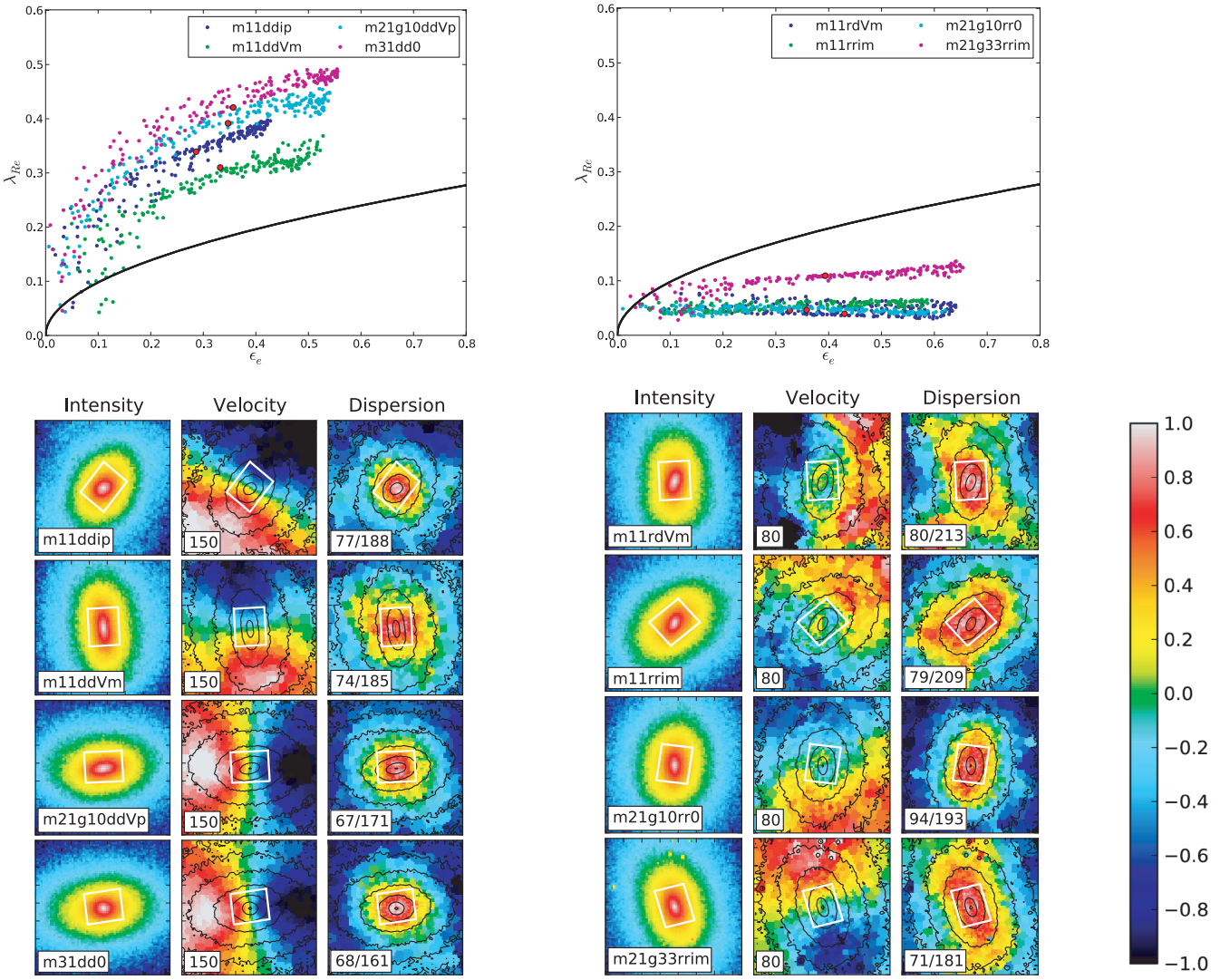

Figure 3. λ_R–ϵ for four fast rotators (left-hand panels) and for four slow rotators with a KDC (right-hand panels). The 200 projections of each merger are represented by a coloured point (see the legend in the figure for the name of the merger); the red point corresponds to the projection with an ellipticity closest to the mean ellipticity. The intensity, velocity and velocity dispersion fields of the previous red point projections are plotted below the λ_R–ϵ diagram. The name of the merger is written in the intensity map, the maximum value of the velocity V_{max} and the minimum/maximum values of the velocity dispersion are written in their respective maps. The colour bar goes from $-V_{max}$ to $+V_{max}$ and can also be used as an indicator for the intensity and the velocity dispersion ('−1' corresponding to the lower value and '1' to the maximum value). The field of view is $15 \times 15\,\mathrm{kpc}^2$ ($15\,\mathrm{kpc} \simeq 6R_e$). The white rectangle indicates a typical field covered by the instrument SAURON and corresponds to a field of $41 \times 33\,\mathrm{arcsec}^2$ for a galaxy at a distance of 20 Mpc; its orientation follows the photometric position angle taken at $3R_e$.

in E+07 (see also McDermid et al. 2006). In both cases, λ_R never reaches the level of fast rotators at very large radii: the mean value of λ_R over the edge-on projections at $3R_e$ is 0.6 for the fast rotators and 0.25 for the slow rotators. The radial λ_R profiles of slow and fast rotators are therefore significantly different at both small and large radii.

The definition of slow and fast rotators seems to robustly disentangle two families of ETGs with different intrinsic properties, with, e.g., the formation of KDCs in slow rotators only. To further understand the influence of various initial parameters, we now explore the impact of the mass ratio, orbital parameters, gas fraction and nature of the spiral progenitors, on the properties of merger remnants.

3.2 Influence of the mass ratio

Fig. 4 shows the λ_R–ϵ diagram for different mass ratios, and different gas fractions in the cases of 2:1 mergers. 1:1 and 2:1 mergers form slow rotators in about 60 per cent of our simulations, the lowest λ_R systems being formed in equal-mass mergers (the fraction of slow rotators directly reflecting the initial orbital parameters; see Section 3.4 and Fig. 5). The formation of slow rotators is unlikely in 3:1 mergers, and does not occur in 6:1 mergers. This is consistent with the conclusions of previous samples of merger simulations (e.g. Naab & Burkert 2003; Bournaud et al. 2004; Jesseit et al. 2009). Bournaud et al. (2004) showed that spheroid-dominated galaxies with little rotating disc components could be formed only during the so-called 'major' mergers (1:1–3:1), while 'intermediate' mergers

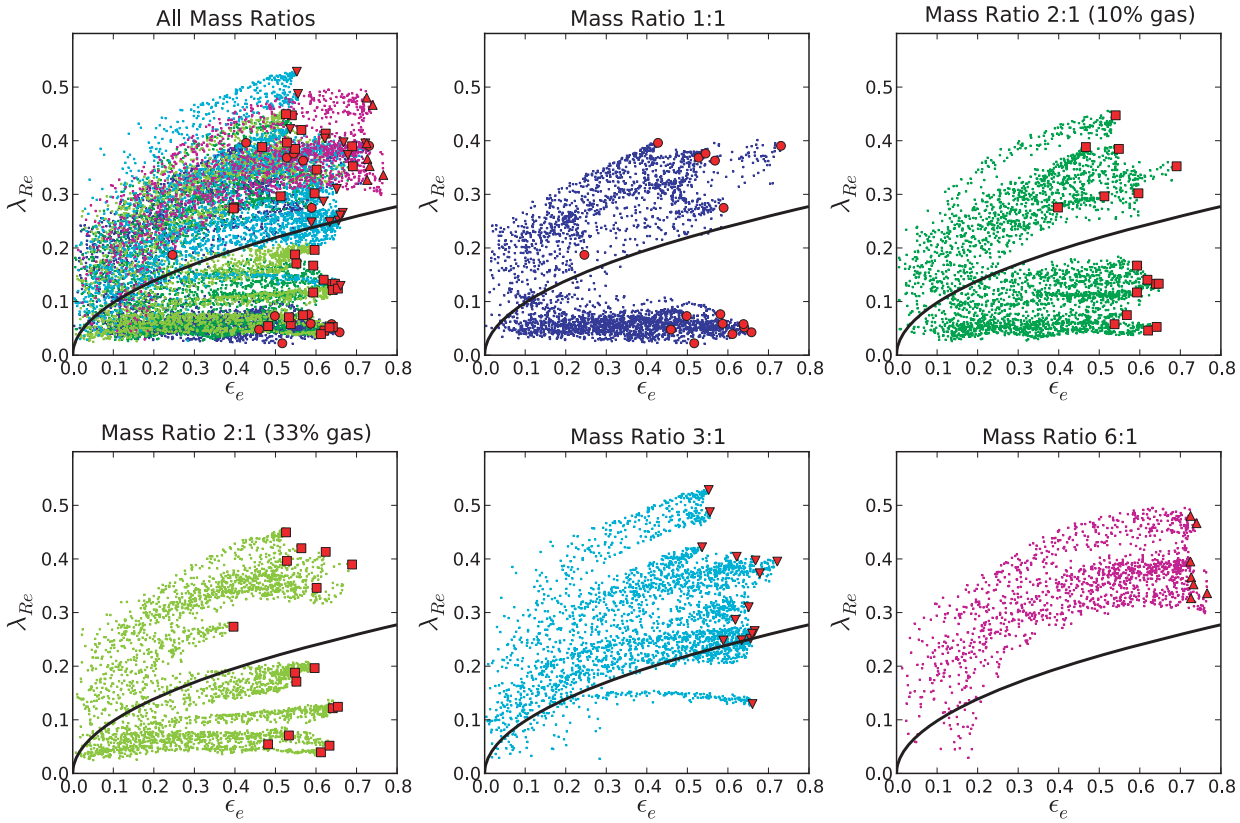

Figure 4. λ_R–ϵ diagram for all simulations of binary mergers of disc galaxies. Top left: all projections of all mass ratios as in Fig. 2; colours correspond to the different mass ratios. Top middle: all projections of merger remnants for mass ratio 1:1. Top right: all projections of merger remnants for mass ratio 2:1 with 10 per cent of gas. Bottom left: all projections of merger remnants for mass ratio 2:1 with 33 per cent of gas. Bottom middle: all projections of merger remnants for mass ratio 3:1. Bottom left: all projections of merger remnants for mass ratio 6:1. The red symbols are for the projection which maximizes the ellipticity for a given remnant. The limit defining the slow/fast categories from ATLAS^{3D} is plotted as the solid black line.

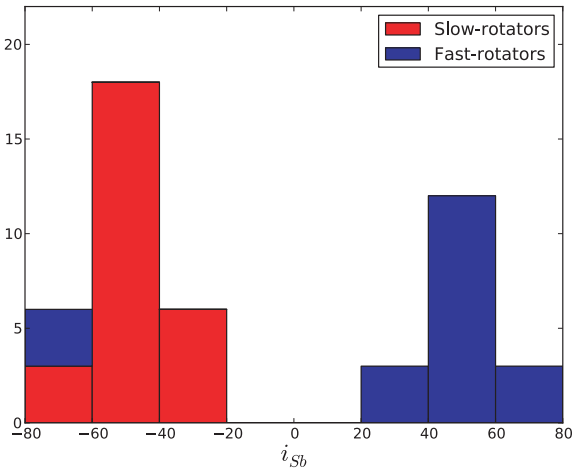

Figure 5. Fraction of slow/fast rotators as a function of the inclination of the main progenitor with respect to the merger orbital plane for mass ratio 1:1, 2:1g10, 2:1g33. The negative inclination occurs when the spin of the Sb progenitor and the spin of the orbital angular momentum are anti-parallel, so that -25° and 25° represent the same inclination for the galaxy but on retrograde orbit.

with mass ratios between 4:1 and 10:1 did not perturb the galaxies much from the initial disc-like morphology and kinematics. Naab & Burkert (2003) found that mass ratios of 3:1 and above formed discy systems. Our present conclusions therefore confirm these results, but with a larger and higher resolution sample of simulations and new analysis parameters.

3.3 Influence of the gas fraction

2:1 mergers were simulated with gas fractions of 10 and 33 per cent. Both subsamples show similar distributions of λ_R, ϵ and presence of a KDC. The gas fraction thus seems to have no major impact on the global properties of the merger remnants, although we did not explore the context of very high-redshift mergers ($z \sim 2$ and above) which could involve extreme gas fractions, e.g., above 50 per cent (Daddi et al. 2010; Tacconi et al. 2010). Mergers with very low gas fractions ($f_{\rm gas} \sim 0$ per cent) should not be associated with spiral-like progenitors, which is the topic of the present section, but with ETG-like progenitors (see Section 4).

A possible cause for the observed similarities between the remnants with 10 and 33 per cent is early gas consumption in the spiral progenitors. If the spirals with 33 per cent of their mass in gas transform most of this gas into stars before the coalescence, this could potentially lead to an actual merger with roughly 10 per cent of gas. We thus investigated how gas consumption proceeds in the progenitors before the merger for both samples (10 and 33 per cent of gas). We first check whether or not the gas consumption is altered by differences in the duration of the merger in the two samples. This is not the case as only the gas fraction is varied, not the orbits: for both samples, the mean time $t_{\rm coal}$ from the start of the simulation to the coalescence is $t_{\rm coal} \simeq 7 \times t_{\rm dyn}$ with the dynamical

time $t_{\rm dyn} \sim 100$ Myr. We then explore the consumption of the gas before the passage at the first pericentre, i.e. when the gravitational force did not have time yet to strongly perturb the progenitors. During that period, the spirals with 10 and 33 per cent of their baryonic mass in gas respectively consume on average 11 and 14 per cent (with a maximum of 17 per cent) of their gas (representing ∼1.1 and 4.6 per cent with a maximum of 5.6 per cent of the total initial baryonic mass). The available gas after the pericentre is then, on average, ∼9 per cent and ∼28 per cent for spirals with initial gas fractions of 10 and 33 per cent. The spiral progenitors are thus still very different when the merger occurs and the similarities between the two subsamples cannot be attributed to a different consumption of gas before the merger.

One could a priori expect that a relatively high gas fraction eases the immediate re-building of massive rotating disc components during or soon after the merger. A few studies suggested that gas-rich mergers could form discy fast rotating systems, or even spiral galaxies (e.g. Springel & Hernquist 2005; Robertson et al. 2006; Hopkins et al. 2009). The relatively stable morphology and kinematics of the 2:1 merger remnants with 10 and 33 per cent of gas could a priori seem conflicting with these earlier results: the value of $\lambda_{\rm R}$ at $1R_{\rm e}$ averaged over all 2:1 mergers varies only from 0.17 to 0.19 when the gas fraction is increased from 10 to 33 per cent and the average value of the ellipticity ϵ varies from 0.39 to 0.38. Actually, a separate study by Bournaud et al. (2010) shows that a high gas fraction does not easily re-form massive and extended disc components in major mergers. This occurs provided that most of the ISM is modelled as a cold medium supported by supersonic turbulence, which is the case in our present sticky-particle simulations[3] and in the AMR models of Bournaud et al. (2010), rather than being supported by a high thermal pressure as it is often the case in existing SPH simulations. This probably explains the differences between our results and the published works mentioned above.

3.4 Influence of orbital parameters

We now examine, for mergers with mass ratios 1:1 and 2:1 which form the majority of slow rotators, how the orbital parameters influence or determine the slow/fast nature of the merger remnant and the associated presence/absence of a KDC.

Fig. 5 shows the distribution of fast and slow rotators as a function of the orbital inclination/orientation with respect to the Sb progenitor galaxy for the 1:1 and 2:1 merger remnants. We remind the reader that the Sb progenitor is the 'main' (most massive) progenitor in the 2:1 mergers. Mergers with a direct (prograde) orbit with respect to the Sb progenitor all produce fast rotators. Mergers with a retrograde orbit with respect to the Sb progenitor almost exclusively produce slow rotators regardless of the spin of the Sc galaxy. The formation of a slow rotator may then be a likely event in a 1:1 or 2:1 merger of spiral galaxies: if the main requirement is to have a retrograde orbit for the main progenitor, the relative fraction of slow and fast rotators should directly reflect the spin distribution of the progenitors (with respect to the orbit; Fig. 4).

These conclusions are further assessed in Fig. 6: it presents the average $\lambda_{\rm R}$ value as a function of the orbital orientation for both progenitor galaxies (i.e. *dd*, *rd* and *rr* orbits) for all mass ratios. It shows that, while *rr* orbits result in a somewhat lower angular momentum at $1R_{\rm e}$ than *rd* orbits (or similar for 1:1 and 6:1 mass ratios), most of the angular momentum removal is already obtained for *rd* orbits, where the orbit is *r*etrograde for the main Sb progenitor but *d*irect (prograde) for the Sc companion.

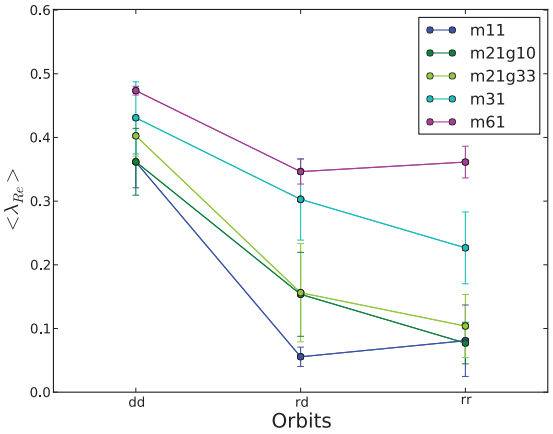

Figure 6. Average $\lambda_{\rm R}$ as a function of the spin of the progenitors for the different mass ratios.

Depending on the initial orbital parameters of the system, the redistribution of angular momentum (orbital momentum plus the internal momenta of each progenitor) via violent relaxation occurs differently. Ideally, we could derive a function describing how this redistribution proceeds in a binary galaxy merger, taking into account the various ingredients of that merger (orbital and internal spins, gas fractions, Hubble type of the progenitors, etc). This would have predictive power in terms of the dynamical status of the remnant (slow or fast rotators) and would be a major asset for implementation in, e.g., semi-analytic models of galaxy formation. Considering that the number of initial parameters is vast, one should need more simulations to constrain and determine such function. This is clearly beyond the scope of the present paper.

3.5 Influence of the Hubble type of the progenitor spiral galaxies

We noted from Fig. 5 that having the main progenitor prograde or retrograde largely determines the fast or slow rotator nature of the merger remnant, while the orbit orientation with respect to the companion has a weaker effect. This is expected for unequal mass mergers, and in particular for 6:1 mass ratios, where the companion mass and momentum are naturally much lower than those of the main progenitor. This is, however, more surprising for 1:1 mergers. Indeed, these equal-mass mergers end-up with a relatively similar $\lambda_{\rm R}$ as long as the Sb progenitor has a retrograde orientation, regardless of the orientation of the Sc progenitor.

This could be the consequence of a 'saturation' effect: the final angular momentum of the merger remnant could be dominated in the centre by one retrograde galaxy with the other (retrograde) galaxy contributing very little. However, the central properties of merger remnants which exhibit relatively high angular momentum obtained via a prograde orientation of the Sb progenitor show little variation whether the Sc progenitor is on a prograde or retrograde orientation. This suggests that the Sb and Sc progenitors do not have symmetric roles in determining the properties of the merger remnant. We first examined whether or not this is an artefact from the initial positioning of the two spiral galaxies in the simulation box and/or the initial orientation of their spin axis with respect to

[3] A difference being that turbulence dissipation in local shocks is 'subgrid' in sticky-particle models, while it is explicitly captured in high-resolution AMR models.

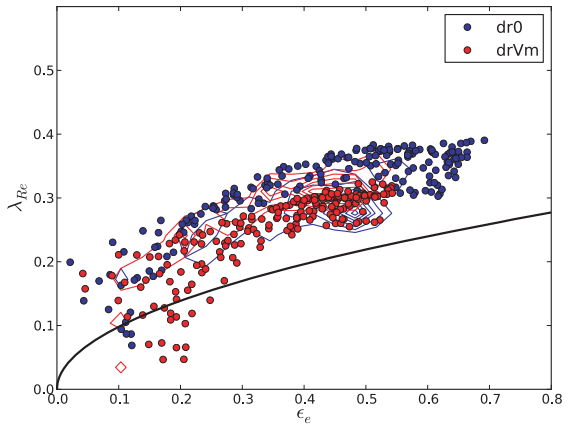

Figure 7. λ_R–ϵ diagram for the *m11dr0* (in blue) and for the *m11drVm* (in red). The contours represent the distribution of the 200 projections of the *m11dd0* (in blue) and *m11ddVm* (in red) simulations.

the numerical grid. To test this, we reversed the initial positioning of the Sb and Sc progenitors and changed the grid orientation in a re-simulation of the *m11rd0* merger: we observe no significant difference in the merger remnants. This confirms that our results do not depend on the simulation box size and grid orientation.

We then simulated mergers in which the Sb progenitor is on a direct orbital orientation, and the Sc progenitor is on a retrograde orientation, i.e. *dr* mergers – so far our sample comprised only *rd* mergers with a retrograde Sb and a direct Sc progenitor. Given that the *m11rd0* and *m11rdVm* orbits resulted in quite typical slow rotators, we performed the corresponding *m11dr0* and *m11drVm* simulations. The λ_R–ϵ profiles are shown in Fig. 7. The *m11dr0* and *m11drVm* remnants are fast rotators, relatively typical compared to the fast rotators produced on *dd* orbits. The outputs of *dr* and *rd* orbits are therefore widely different. This shows that while the angular momentum of a merger remnant largely depends on the total available (baryonic) angular momentum, i.e. the sum of the orbital angular momentum and the internal spin of each progenitor galaxy, the Hubble type of the progenitor galaxies – i.e. their central concentration and dynamical stability – has a significant impact. A retrograde orbit around an early-type spiral, such as our so-called Sb galaxy, is efficient in producing slow rotators (for 1:1 and 2:1 mergers). A retrograde orbit around a late-type spiral, such as our so-called Sc galaxy, does not significantly impact the angular momentum remaining in the central body of the merger remnant (see Fig. 7 and Section 5.3 for the interpretation).

4 GALAXY REMERGERS

Naab, Khochfar & Burkert (2006b) suggested that mergers of ETGs play an important role in the assembly of massive galaxies. Khochfar & Burkert (2003) have also shown, via simulations in a cosmological context, that the last major merger of bright present-day ETGs ($M_B \lesssim 21$) was preferentially between bulge-dominated galaxies, while those with $M_B \simeq 20$ have mainly experienced last major mergers between a bulge-dominated and a disc-dominated galaxy. This section thus introduces binary galaxy mergers of ETGs, or 'remergers', with the goal to examine the morphology and kinematics of such remnants. The progenitors we used for this analysis are themselves the remnants of binary disc mergers described in the previous sections.

Table 3 details the remergers we have performed. We run simulations for four pairs of progenitors with different orbital configurations (*dd*, *dr*, *rd*, *rr*). The first three pairs have been drawn from simulations with two initial mass ratios and two initial gas fractions, namely m11, m21g10 and m21g33. In these three cases, the orbital configurations that generated the progenitors were kept the same for a given remerger configuration, e.g. for a *dd* remerger orbit we always use progenitors coming from rd0 (primary) and rr0 (secondary) orbits. The progenitors for the fourth pair (fourth remerger set) are m21g10 and a spiral. Velocity maps of all remerger remnants are shown in Figs A6 to A9 in the Appendix.

Fig. 8 presents the λ_R–ϵ diagram for the remergers; the four subplots correspond to the four different types of remergers (rem2x11, rem2x21g10, rem2x21g33, rem21g10+S) and the four colours in each subplots corresponding to the orbit of remerging (*dd*, *dr*, *rd*, *rr*). From the results of binary galaxy disc mergers (see the previous sections), we could presume that the *rr* orbit would produce the slowest rotators of this sample of remergers. In fact, the *dd* cases are the ones to produce the slowest systems for the four different types of remergers. In the *dd* cases of galaxy remergers, both progenitors are slow rotators and hold a KDC. The progenitors acquire angular momentum from the orbit, resulting in merged galaxies with large-scale rotation, and the KDCs have been destroyed. The remnant is classified as a slow rotator but is very close to the dividing line separating slow and fast rotators. The remnant does not present any sign of a KDC and has its photometric and kinematic axis aligned.

In the other cases (*dr*, *rd*, *rr*), the main progenitor is a slow rotator with a KDC and the companion is a fast rotator. During the merger, the main progenitor – with no global rotation – acquires angular momentum from the orbit while the companion – similar to the behaviour of the spiral Sb progenitor – keeps the initial orientation of its spin, the contribution of which determines and dominates the final spin of the remnant. None of these remergers exhibits a stellar KDC: the KDCs which were present in the progenitors have been destroyed and none is created during the merger. The final remnants of these remergers are rounder than binary disc merger remnants and all have regular kinematics. As mentioned, a few of

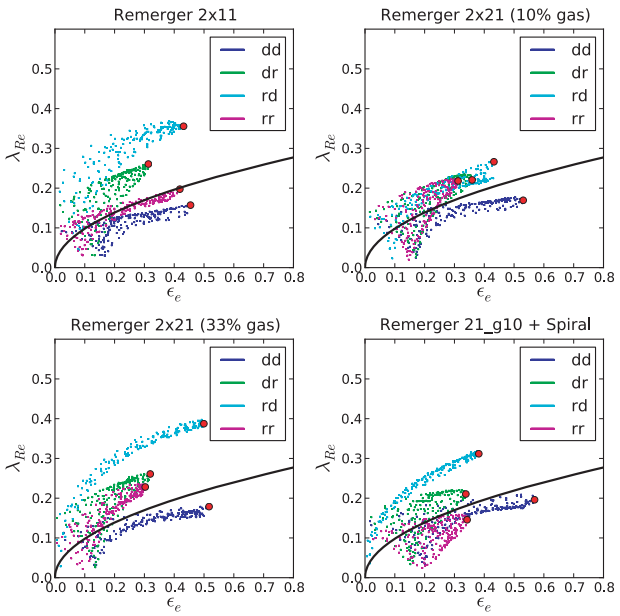

Figure 8. λ_R–ϵ diagram for all projections for all simulations of remergers. The four panels represent the four different remergers, and the four colours in each subplot correspond to the orbit of remerging (*dd*, *dr*, *rd*, *rr*).

these (mostly the *dd*) lie just below the limit between the slow and fast rotators, emphasizing the potential small overlap between the two families (Paper III).

As seen in our sample of galaxy remergers, and in agreement with the results of Di Matteo et al. (2009), slow or non-rotating galaxies can gain central angular momentum through mergers via a transfer of the orbital angular momentum and start to rotate. The final state of a merger remnant is the combination of internal+orbital angular momentum: starting with one or two slow rotators can thus lead to a rotating merger remnant. To form a round slow rotator via ETG mergers, one should need two fast rotators on a favourable (e.g. *rr*) orbit. Repeated minor mergers may preserve the initial KDC of the initial ETG and heat the external parts of the galaxy (Bournaud et al. 2007; Qu et al. 2010): this could end up with a round slow rotator, but this scenario has not been tested yet.

5 PROPERTIES AND FORMATION MECHANISMS FOR KDC VIA MAJOR MERGERS

In this section, we focus on the processes involved in the formation of a KDC in our simulations, and we thus examine the relative contribution of the different components, namely the old stars, the young stars and the gas associated with the KDC observed in the merger remnant.

5.1 The contribution from old stars

To probe the contribution of the old stars in the slow rotator remnants with a KDC, we have separated the old stars which belong to the Sb progenitor from the ones of the Sc companion. The intensity and velocity fields of six analysed cases (m11, m21g10, m21g33 with *rd* orbit and m11, m21g10, m21g33 with *rr* orbit) are shown in Fig. 9. The projections used in that figure have been selected to emphasize the respective contributions of the progenitors in the final remnant and do not specifically correspond to edge-on or face-on views of the galaxy.

There seem to be two qualitatively different types of KDCs which can in fact be associated with different initial orbits. In the *rd* cases, a KDC is visible within $1R_e$ and results from the luminosity-weighted average of two counter-rotating stellar systems. In the *rr* orbits, the KDC is more prominent and extended, and is visible in the *individual* contributions of both progenitors, at least for the 1:1 mergers. This can be understood by following the Sb and Sc progenitor in turn.

The Sb progenitor remains, within the central region, mostly unaffected by the merger, even for large mass ratios (1:1). This is true except at $R < R_e$ for the *rr* orbit: when the Sc companion has a negative spin (with respect to the orbit) the Sb progenitor is more severely affected. This is consistent with the picture developed by Renaud et al. (2009) which suggests that retrograde galaxy orbits allow more material to be available for later interactions when galaxies get closer to each others.

The Sc progenitor is, in stark contrast with the Sb progenitor, almost entirely disrupted during the merging event and will basically adopt part of the orbital angular momentum (the rest being transferred to the dark matter component) and its sign. The final contribution of the Sc progenitor in the remnant therefore mostly reflects that choice of orbit, which was assumed as prograde (positive) as a reference. When the Sc progenitor itself is on a prograde orbit, this will add up to produce a rapidly rotating stellar component to the remnant. When the Sc progenitor is on a retrograde orbit, and considering that the close interaction time between stars of the Sc and the global potential of the Sb is then shortened (Renaud et al. 2009), some stellar material with the initial angular momentum sign will remain in the remnant potentially producing a rather large stellar KDC (from old stars).

We can therefore naturally expect a KDC to form as soon as the Sb progenitor is on a retrograde orbit, due to the superposition of a positively rotating contribution from the companion, and the counter-rotating stellar contribution of the main Sb progenitor. When the Sc is on a retrograde orbit, it more violently affects the Sb progenitor which then exhibits a KDC. The Sc is then also transformed into a stellar system with rather disturbed and complex dynamics resulting from the superposition of the orbital wrapping (following the galaxy orbit) and the initial angular momentum of the stars (in the opposite sense).

This process is valid for both the 1:1 and 2:1 mergers. However, the Sc companion in unequal mass mergers has obviously a smaller influence on the Sb progenitor and is itself more easily destroyed which explains why it appears as having fully adopted the sign of the orbital angular momentum vector. This is nicely illustrated in Fig. 9. In the case of a 2:1 *rr* merger, the two contributions have roughly the same mass profiles within the central kpc. The velocity map of the remnant is then composed of the superposition of the counter-rotating component of the Sb progenitor and the contribution from the Sc companion. At larger radii ($r > 1$ kpc), the Sb galaxy is dominant in mass and leads the velocity field of the merger remnant. An apparent KDC is then visible in the merger remnant. The small ($\sim$1 kpc) decoupled core in the centre of the Sb progenitor is also smaller than in 1:1 mergers because the companion is lighter and does not affect the central stars of the Sb progenitor much. However, as also pointed out in the 1:1 merger cases, the decoupled core is larger than in the *rd* case as the mass of the companion falling in the centre is bigger.

We can now easily extend this analysis to the *dd* and *dr* cases which produce fast rotators. In the case of a *dd* orbit, the two spins of the progenitors are aligned with the spin of the orbital angular momentum. This maximizes the (positive) angular momentum, which naturally produces a flattened fast rotator. The output of the case of the *dr* orbit can be extrapolated from the *rr* case: the Sc companion has a spin anti-parallel with respect to the orbital angular momentum vector. During the approach, the companion is violently disturbed and its stars (most of them in 1:1 and all of them in 2:1 mergers) merge with the Sb progenitor with the spin of the orbit (and of the Sb progenitor). The final merger remnant is then composed of two components with the same sense of rotation and is then a fast rotator, just slightly rounder than for a *dd* orbit.

5.2 The contribution from young stars and gas

In Fig. 10 we present the velocity fields of the gas and the young stars of the projections used for Fig. 9, the iso-magnitude contours of the old stars being superimposed. We can see that the gas and the young stars share the sense of rotation with the outer part of the final remnants. The gas does not show much sign of a disturbed morphology or kinematics in the centre. The young stars exhibit some misalignments in the very centre of the galaxy; these misalignments being roughly at 90° with respect to the photometric major-axis of the remnant. The gas, and the associated star formation, thus does not play a major role in the KDC itself, although the concentration

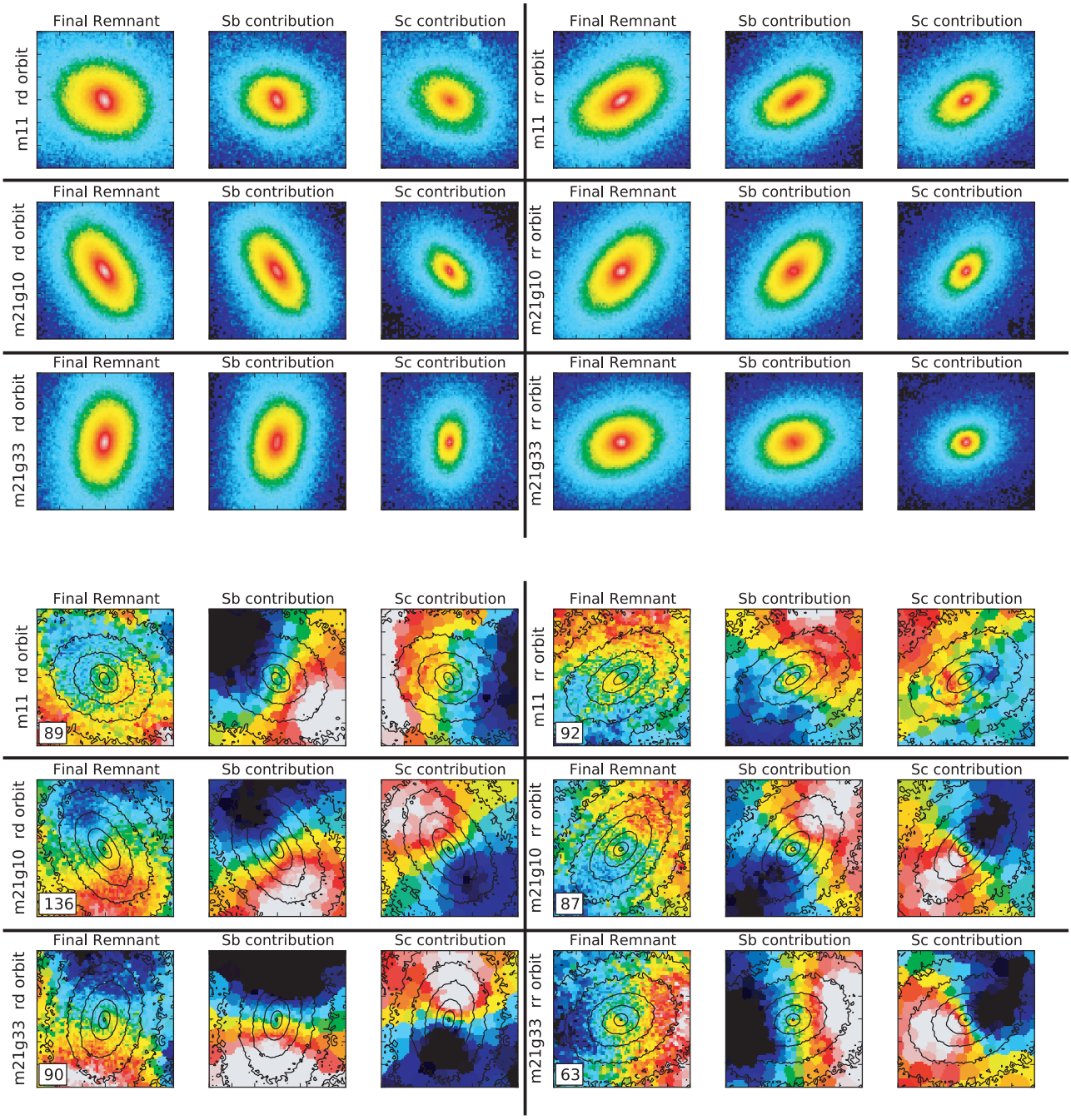

Figure 9. Intensity (three top panels) and velocity (three bottom panels) fields of the old stars for the final merger remnant, for the stars belonging to the Sb progenitor in the remnant and for the stars belonging to the Sc companion in the remnant. The cuts in magnitude and velocity are computed from the final remnant and applied to the Sb and Sc progenitor contributions. The field of view for each panel is $15 \times 15\,\mathrm{kpc}^2$.

of gas and young stars in the central part of the merger remnant bring an additional central density which could influence the evolution of the KDC.

A small (∼1 kpc) KDC is observed in the map of the young stars for the m11rr case (Fig. 10). These young stars, formed in a burst of star formation near the pericentre, are thus subjected to violent relaxation, as are the old stars. Part of the young and old stellar populations of the two progenitors end up in two counter-rotating discs (see the previous section): forming, under certain conditions, a central KDC. Galaxies with a young KDC counter-rotating with respect to the gas supply are actually observed in the ATLAS^{3D} sample (McDermid et al., in preparation).

5.3 Summary

The KDCs in the merger remnants are mostly seen in the old stars, with only a weak signature in the young stars (none in the gas). Moreover, most of the KDCs formed in the major mergers (1:1, 2:1) do not correspond to physically distinct stellar components (see also the study of van den Bosch et al. 2008), except in the

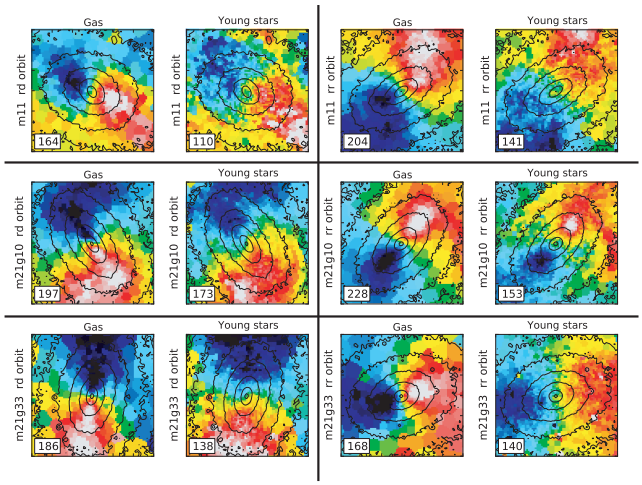

Figure 10. Velocity fields of the gas and the young stars in the final merger remnant, iso-magnitude contours of the old stars of the final remnant are superimposed. The field of view for each panel is $15 \times 15\,\mathrm{kpc}^2$.

case of 1:1 binary disc mergers on an *rr* orbit. These 'apparent' KDCs result from the superposition of two counter-rotating stellar components where one disc is dominating the mass profile in the centre while the second disc is dominating outwards. This scenario seems to hold even when the two progenitor discs have the same sense of rotation but with a spin which is retrograde with respect to the orbital angular momentum. The formation of an apparent counter-rotating core (CRC) with two initial retrograde progenitors has also been probed by Balcells & Quinn (1990) in a 5:1 merger of oblate ETGs: the companion adopts the sign of the orbital angular momentum during the merger to form a CRC when the two galaxies merge. The physical process invoked to form CRCs in Balcells & Quinn (1990) appears consistent with the one witnessed in the present study, although we only form here CRCs in remnants of major (1:1 or 2:1) mergers.

As pointed out in Section 3.5, the two progenitors have a different influence on the output of the merger. Our so-called Sb progenitor is more concentrated and dynamically stable, and most of its stars keep their original orientation during the merger. The so-called Sc progenitor is colder, less concentrated and responds more efficiently to potential disturbances.

Our study on the formation of the KDCs in binary mergers of disc galaxies should therefore be completed by probing mergers with various morphological types, e.g. Sb–Sb or Sc–Sc. The detailed role of the Hubble type for disc progenitors in galaxy mergers is an important issue which will be examined in a future study.

6 RECENT STUDIES ON SIMULATED BINARY MERGERS AND THE FORMATION OF KDCs

We have focused our analysis on the central part of the merger remnants to study in details the formation of the slow and fast rotators (and the formation of the KDCs) and here, we specifically compare our results with two other sets of simulations, namely the work of Jesseit et al. (2009) and Hoffman et al. (2010). They have both performed a suite of simulations using the TreeSPH code GADGET-2 (Springel 2005) with a gravitational softening length of 140 pc. In these simulations, Hoffman et al. (2010) included radiative heating and cooling, star formation, feedback from supernovae and active galactic nuclei and used a total of 4×10^5 particles while Jesseit et al. (2009) 'only' included star formation and stellar feedback but with a total of $\sim 10^6$ particles. We discuss in the following some relevant differences between these studies and ours.

Jesseit et al. (2009) emphasized the formation of slow and fast rotators with their sample of simulations. They have simulated binary mergers of disc galaxies with mass ratios from 1:1 to 4:1 as well as galaxy remergers. We find some significant differences with their results.

(i) 75 per cent of their 1:1 mergers, but only 10 per cent of their 2:1, are slow rotators. This can be compared with 60 per cent for both 2:1 and 1:1 mergers in our sample.

(ii) Overall, their merger remnants are rounder than ours. Their progenitors have $\epsilon < 0.5$, their slow rotators have $\epsilon < 0.4$ and their dry remnants are flatter but do not have $\epsilon > 0.6$. The distribution of λ_R and ϵ for their fast rotator remnants is consistent with the fast rotators described in the present paper.

(iii) The ellipticity and λ_R distributions of their 1:1 disc–disc merger remnants are 'hardly distinguishable' from their ETG–ETG merger remnants. From our sample, the difference is very clear, our ETG–ETG merger remnants are rounder and are classified as fast rotators, and we do not produce slow rotators with very low λ_R values from remerging of disc binary mergers.

These differences could mainly be explained by variations in the initial parameters of the disc galaxies. The progenitors in Jesseit et al. (2009) have a more massive bulge ($B/T = 1/4$, as compared to $B/T = 1/5$ and 1/8 for our study), and their bulges are non-rotating: this may produce rounder remnants. These remnants are also classified as slow rotators, which may be again linked with the absence of rotation of the bulges in their progenitors.

The distance between the two progenitors at the pericentre is about two disc scalelengths ($\sim$7 kpc) in Jesseit et al. (2009) while this distance is about 10 to 25 kpc (depending on the mass ratio) in our study. The lower angular momentum of orbits induced by the lower pericentric distance may also affect the merger remnants. In the present study, we have also simulated binary mergers with an impact parameter R decreased from 60 to 35 kpc. There is no significant difference in the shapes and kinematics of the merger remnants we obtain, for all mass ratios and initial spins of the progenitors, when the value of R is decreased. Other simulations with even lower pericentre distances (e.g. with impact parameters $\lesssim$10 kpc as in Hoffman et al. 2010) should be considered for further comparison, but this is outside of the scope of this paper. Orbits with large impact parameters and pericentric distances, as in our study, seem statistically more representative of hierarchical merging in ΛCDM context (Khochfar & Burkert 2006). However, the presence of an external gravitational field (in dense environment) may significantly impact the orbit of the two progenitors, decreasing the pericentric distance (Martig, private communication): this will be examined in more detail in a forthcoming paper.

Hoffman et al. (2010) have simulated binary mergers of disc galaxies of mass ratio 1:1 at different gas ratio (from 0 to 40 per cent of gas). Again, there are several differences between their results and ours.

(i) From 0 to 10 per cent of gas, their remnants are all slowly rotating. They do not have KDCs; the slow rotator galaxies are dominated by box orbits or by minor-axis rotation. With 15 and 20 per cent of gas, most of their remnants have a KDC. When reaching 30 and 40 per cent of gas, their remnants are all fast rotators. They do not mention any trend between the initial condition of merging (e.g. the orientation of the discs) and the formation of slowly rotating ETG.

(ii) Their KDCs are small discs of young stars coming from the gas in rotation in the centre. When the fraction of gas is increased, the size of the final disc of gas – and thus the disc of young stars – is also increased and it creates a fast rotator. Their fast rotators are purely dominated by the young stars created in this large disc of gas in rotation. In our sample, the KDC is an apparent KDC (except for the 1:1 merger with *rr* orbits) and is seen only in the old stars. The gas does not show any sign of counter-rotation. Our KDCs do not depend on the gas ratio, as we do not find any significant difference between the remnants with 10 or 33 per cent of gas.

Hoffman et al. (2010) have used pure stellar discs (i.e. without a stellar bulge or spheroid) as progenitor galaxies, and a low impact parameter of 7.1 kpc (and thus a lower pericentric distance). These initial conditions are far from ours and lead to a very different merging process. We speculate that, as the orbit leads to a more rapid and direct collision, the two discs are destroyed and strongly influenced by violent relaxation and are not expected to keep track of the original disc dynamics (except at large radii as pointed out in their paper). This may explain why none of their low gas fraction mergers shows signs of rotation around the short-axis of the remnants.

The treatment of the gas and the resolution used for the simulations are also different between this study and the one presented here. Bois et al. (2010) showed that at a high resolution, thinner gas structures are resolved during the merger, which can result in structured and clustered star formation. These local density peaks are accompanied by rapid variations of the gravitational potential, which help scatter stellar orbits and evacuate the angular momentum. A gas-free and a gas-rich merger should differ not only with the re-formation of a disc of gas in the centre of the remnant as seen in Hoffman et al. (2010), but also at all radii with different stellar orbits (see also Bournaud et al. 2010). These results emphasized the need for high spatial and mass resolution (see also Bois et al. 2010; Teyssier, Chapon & Bournaud 2010; Powell et al. 2011) and for realistic physical inputs: e.g. the treatment of the gas with models capable of resolving the main dense gas clouds/SF regions (see Governato et al. 2009, in a cosmological context).

7 COMPARISON WITH OBSERVATIONS

We compare here directly our sample of merger remnants (binary mergers and ETG remergers) with the sample of 260 galaxies observed in the context of the ATLAS^{3D} project (Paper I). For that purpose, we first use the λ_R–ϵ diagram, and also compare the distribution of alignments between the photometric and kinematic axes.

7.1 The λ_R–ϵ diagram

Fig. 11 shows the λ_R–ϵ diagram for the 260 galaxies of the ATLAS^{3D} sample (extracted from Paper III) and presents the distribution of projections for the simulated spiral progenitors, remerger remnants and merger remnants of binary disc galaxies. It also presents the distribution of projections for our merger remnants of binary disc galaxies weighted by the probability of the galaxy–galaxy merger rate as a function of the mass ratio in ΛCDM. From Hopkins et al. (2010) for a galaxy of mass $10^{11}\,M_\odot$ (i.e. with the mass of our main progenitor), if P is the probability of having a 1:1 merger, the probability to have a 2:1 merger (respectively 3:1 and 6:1) is $4P$ (respectively $6P$ and $9P$). The lower mass ratios are favoured, so does the formation of fast rotators via a binary galaxy merger.

By looking at where the observed ATLAS^{3D} galaxies and our sample of galaxy mergers lie in such a λ_R–ϵ diagram, we can make

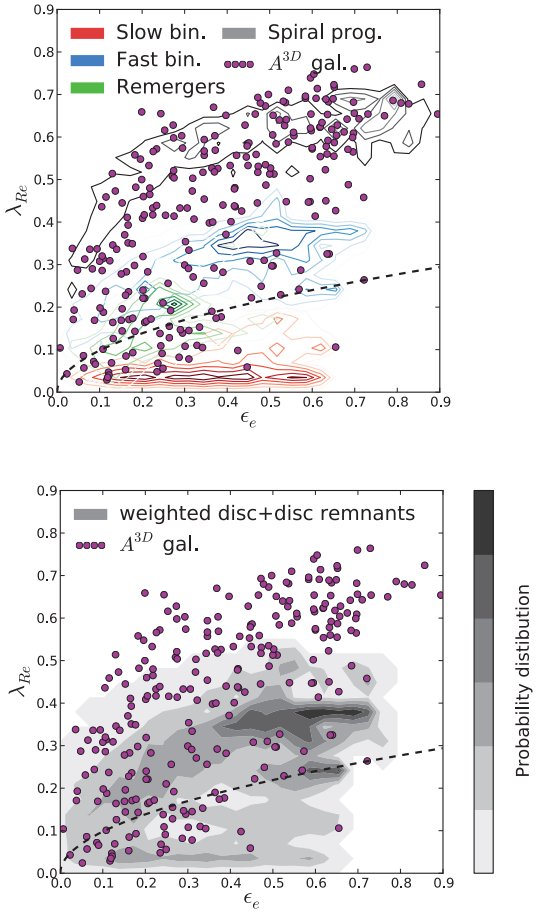

Figure 11. λ_R–ϵ diagram for the 260 galaxies of the ATLAS^{3D} sample (shown as dots) compared to our simulation sample. The dashed line corresponds to the limit defining the slow and fast rotators. Top: the contours represent the distribution of projections of the simulated fast rotator disc remnants in blue, slow rotator disc remnants in red, remerger remnants in green and spiral progenitors in black. Bottom: the contours represent the distribution of projected remnants (slow+fast) of disc mergers statistically weighted depending on the likelihood of its mass ratio (see the text for details).

a first rough assessment of the relevance of binary disc mergers and remergers for nearby ETGs:

(i) For high values of λ_R (∼0.5–0.8), the distribution of ATLAS^{3D} galaxies coincides in fact with the distribution of our progenitors; this has been also pointed out in Jesseit et al. (2009). These local galaxies often contain a bar and are consistent with disc galaxies. These could be disc galaxies which have evolved via various internal processes – at high redshift (e.g. Elmegreen, Bournaud & Elmegreen 2008; Dekel, Sari & Ceverino 2009) and/or at low redshift (Athanassoula & Bureau 1999) – and through accretion of gas or very small companions (Toth & Ostriker 1992; Martig & Bournaud 2010; Moster et al. 2010).

(ii) For intermediate values of λ_R (∼0.25–0.5), the ATLAS^{3D} galaxies are closer to the fast rotator merger remnants. These observed ETGs could thus be the remnants of a merger between a spiral galaxy and a companion with a mass ratio from 10:1 to 1:1 (see e.g. Bendo & Barnes 2000; Cretton et al. 2001; Naab & Burkert 2003; Bournaud et al. 2005; Naab & Trujillo 2006).

(iii) In the ATLAS^{3D} sample, we find ∼30 galaxies with $\lambda_R < 0.25$ classified as fast rotators. These galaxies have rather small

ellipticities: some of these therefore may be consistent with the remnants of a binary merger of disc galaxies viewed face-on, but this cannot hold for the full set of low λ_R fast rotators. As seen in Fig. 11, the result of a major remerger can form a galaxy with a relatively low intrinsic ellipticity and low λ_R values and can better account for these galaxies. A remnant of a major binary merger of spirals followed by mergers of smaller companions, or the fast evolution of galaxies in groups (see e.g. Konstantopoulos et al. 2010) may also lead to a similar output.

(iv) The comparison with the observed slow rotators is less evidential. In the context of the subclasses of slow rotators defined in Paper II, we can emphasize the following items. Observed non-rotators are among the most massive objects in the ATLAS^{3D} sample (Papers I and III) and very probably have a complex merger history (Nieto, Bender & Surma 1991; Tremblay & Merritt 1996), clearly beyond the simple picture provided by the binary mergers described here. Galaxies observed to exhibit KDCs all have apparent $\epsilon < 0.4$: as already emphasized, the slow rotator remnants obtained in our sample of simulations are much too flat comparatively. This implies that only a few of the observed slow rotators could have been simply formed via binary mergers of disc galaxies, and these would in addition need to be viewed at relatively high inclination. Slow rotators could therefore be the result of a single major merger but then with significantly more violent initial conditions (e.g. with a very small impact parameter; Duc et al., in preparation) or must have experienced further interactions: a sequence of small satellite mergers may produce rounder remnants and at the same time preserve the KDCs. Such accretion of low-mass objects should be much more frequent than major mergers and are therefore expected (see e.g. Khochfar & Silk 2006; Naab et al. 2007; Bournaud, Jog & Combes 2007; Genel et al. 2008, 2010; Naab, Johansson & Ostriker 2009; Hopkins et al. 2010; Oser et al. 2010; Qu et al. 2010; Abadi et al. 2010, ΛCDM models).

(v) We can probably account for 2σ galaxies with our sample of simulations. All the observed 2σ galaxies have $\epsilon > 0.3$ and their properties (see Papers II and III) indicate that they could have been formed via a single binary merger (see also Balcells & Quinn 1990; Hernquist & Barnes 1991; Balcells & González 1998; Barnes 2002; Jesseit et al. 2007; Crocker et al. 2009). Fig. 12 shows three simulated merger remnants (formed with 1:1, 2:1 and 3:1 mergers) which resemble the observed 2σ galaxies. The remnants formed via 1:1 and 2:1 mergers are classified as slow rotators and present a KDC while the remnant formed with a 3:1 merger is a fast rotator (without KDC) but staying close to the limit defining these two populations. This picture is consistent with the ATLAS^{3D} observations where 2σ galaxies are found in both families of ETGs.

7.2 Photometric and kinematic alignments

Based on the Franx, Illingworth & de Zeeuw (1991) definition, we calculate the kinematic misalignment angle Ψ as the difference between the measured photometric and kinematic position angles

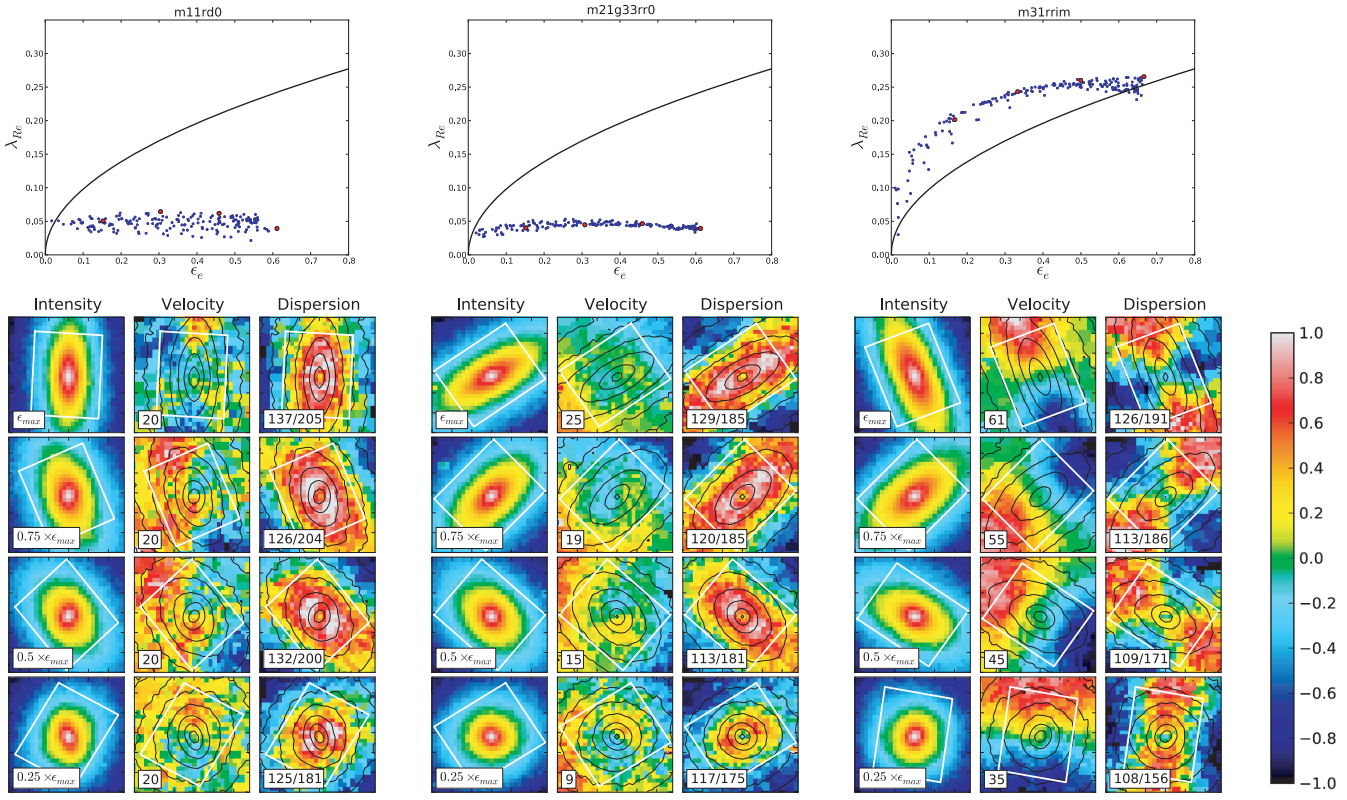

Figure 12. Three simulated 2σ-like galaxies: a 1:1 slow rotator (left), a 2:1 (with 33 per cent of gas) slow rotator (middle) and a 3:1 fast rotator (right). The top panels represent the λ_R–ϵ diagram for the 200 projections plotted as blue dots, the red points correspond to the projection with the maximum ellipticity ϵ_{max} and the projections corresponding to $0.75 \times \epsilon_{max}$, $0.5 \times \epsilon_{max}$ and $0.25 \times \epsilon_{max}$. The lower panels show the intensity, velocity and velocity dispersion maps of the red point projections. The projection is written in the intensity map; the maximum value of the velocity and the minimum/maximum values of the velocity dispersion are written in their respective maps. The colour bar goes from $-V_{max}$ to $+V_{max}$ and can also be used as an indicator for the intensity and the velocity dispersion. The field of view is $6 \times 6\,kpc^2$ ($6\,kpc \simeq 2.5R_e$). The white rectangle indicates a typical field covered by the instrument SAURON and corresponds to a field of 41×33 arcsec^2 for a galaxy at a distance of 20 Mpc; its orientation follows the photometric position angle taken at $3R_e$.

taken at three effective radii (see also Paper II) as

$$\sin\Psi = |\sin(\mathrm{PA_{phot}} - \mathrm{PA_{kin}})|.$$

The measurement of this quantity at large radii minimizes the impact of central decoupled structures such as a KDC and bar. Ψ is defined between two observationally related quantities, and it approximates the true kinematic misalignment angle which should be measured between the intrinsic minor-axis and the intrinsic angular momentum vector. Ψ can range from 0° to 90° (the use of sin removes additional differences of 180° between $\mathrm{PA_{phot}}$ and $\mathrm{PA_{kin}}$).

This analysis has been made for the sample of the 260 ATLAS^{3D} galaxies in Paper II. The regular velocity pattern galaxies (i.e. fast rotators) are mostly found at small Ψ values, and the galaxies with complex kinematic structures (non-rotators, NRV, 2σ and KDC galaxies) often exhibit strong misalignments between the photometry and kinematics.

Our simulations are in good agreements with these observational results. The top panel of Fig. 13 shows the histogram of the kinematic misalignment angles for all projections of all binary merger remnants. The fast rotators have 60 per cent of their projections in the first bin with $\Psi < 5°$, with another 17 per cent with $5 < \Psi < 10°$, and 88 per cent of the projections have $\Psi < 20°$. The slow rotators for the 2:1 mergers have, respectively, 42, 15, 82 per cent of their projections in these domains, respectively, while the slow rotators associated with 1:1 mergers are distributed homogeneously from 0° to 90°. Our fast rotator remnants should thus be considered as perfectly aligned: the spin axis of the stellar component is the photometric short-axis. The slow rotators associated with 2:1 mergers are also relatively well aligned: the most massive progenitor (the Sb spiral in this study) dominates the velocity rotation, and the galaxy remnant remains flat and disc-like. The slow rotators formed in 1:1 mergers show significant misalignment: the two progenitors end up contributing to counter-rotating stellar components which almost cancel any central rotation around the photometric minor-axis. The rotation is then dominated by the kpc-size KDC and by rotation along the photometric minor-axis at larger radii (Hoffman et al. 2010). These results are confirmed when selecting the projections which maximize the ellipticity (i.e. the edge-on projection) of the merger remnants (see also Figs A1 to A5 in Appendix A for the corresponding velocity maps): the edge-on projections of the fast rotators are always aligned with $\Psi < 5°$ (except for the merger remnant *m11rrip*), while some 2:1 slow rotators show significant misalignments and all 1:1 slow rotators do.

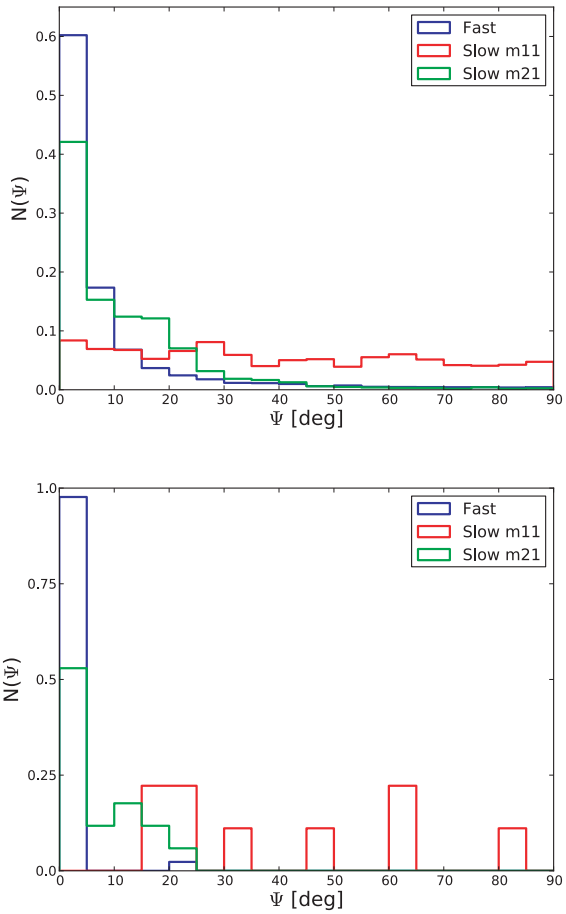

Figure 13. Top: histogram of the kinematic misalignment angle (in degree) for all projections of the merger remnants. The *y*-axis is normalized to the total number of projections per categories: the fast rotators (for mass ratios 1:1 to 6:1) are in blue, the slow rotators of mass ratio 1:1 in red and the slow rotators of mass ratio 2:1 (both 10 and 33 per cent of gas) in green. The errors on Ψ are within a bin size. Bottom: same histogram but only for the projections which maximize the ellipticity (edge-on view) of the merger remnants.

The same results are found by Jesseit et al. (2009); they have analysed misalignment angles for the oblate, prolate and triaxial simulated merger remnants described in Thomas et al. (2007). Their disc-like oblate system is a fast rotator and has most of its projections with $\Psi < 5°$ while the more disturbed prolate and triaxial remnants show misalignments.

7.3 Summary

The morphology and kinematics of the modelled fast rotators (including the spiral progenitors) are in good agreement with the observed local fast rotators, mainly composed of flat and rotationally supported discs with nearly aligned photometric and kinematic axes. In the context of our sample of simulations, we can exclude the formation of the non-rotators via binary mergers of disc or ETG: these are intrinsically round and thus supported by velocity dispersion alone, properties which are not observed in our sample of merger remnants. The observed galaxies with a KDC shared some properties (misalignments and angular momentum content) with our simulated merger remnants but they are also intrinsically rounder: their formation history is then certainly much more complex than the simple picture of binary mergers of disc galaxies. We can possibly account for the formation of some observed slow rotator galaxies of the ATLAS^{3D} sample, namely the *so-called* 2σ galaxies, with 1:1 or 2:1 mergers: these systems present signatures of the presence of two counter-rotating components (see e.g. van den Bosch et al. 2008). A more detailed comparison, e.g., including $h_{3,4} - v/\sigma$ diagrams, or gas distribution and kinematics, would be required to confirm this result.

8 CONCLUSIONS

We have simulated 70 binary mergers of disc galaxies at an unprecedented resolution for such a sample of simulations. We have studied the effect of different initial parameters on the global properties of merger remnants, varying: the mass ratio (from 1:1 to 6:1), the initial conditions of the mergers (incoming velocity, impact parameter, inclination in the orbital plane), the spins of the progenitors. We have

also simulated 16 binary remergers of galaxies between two binary spiral merger remnants, varying: the mass, the class (slow/fast) of the progenitors and the spin of the initial ETG-like progenitors. We have then compared the properties of our sample of (re)merger remnants with the observed 260 ETGs of the ATLAS^{3D} survey. We have also compared our work with previous established samples of numerical simulations. Our main conclusions can be summarized as follows.

(i) We obtain both fast and slow rotators. In binary mergers, the fast rotators can be observed at all mass ratios while the slow rotators are formed only for mass ratios between 1:1 and 2:1, in agreement with Jesseit et al. (2009). We confirm that the limit separating the two families of ETGs defined by the ATLAS^{3D} survey is meaningful, as our simulated slow and fast rotators present distinct characteristics: the fast (respectively slow) rotators have a high (respectively low) angular momentum content, their photometric and kinemetric position angle are aligned (respectively misaligned), they present (respectively do not present) regular velocity patterns. An important difference is the presence (or absence) of a KDC: none of the fast rotators holds a KDC while most of the slow rotators do.

(ii) The two parameters which constrain the formation of the KDCs are (1) the mass ratio between the initial spirals, as we form a KDC only with 1:1 and 2:1 mergers, and (2) the orientation of the initial spin axis of the earliest-type (Sb) disc progenitor with respect to the orbital angular momentum (its spin has to be anti-parallel). The spin of the later-type (Sc) progenitor has less importance as this galaxy is mostly disrupted during the merging process. For a 1:1 merger, if the two progenitors are retrograde, the KDC is intrinsically decoupled from the external part of the merger remnant. For all other initial conditions leading to the formation of a slow rotator, the KDC is only an apparent KDC formed via the superposition of two counter-rotating discs.

(iii) The Hubble type of the initial spiral progenitors seems to play a prominent part in the formation of slow rotators and additional simulations are needed to further constrain its role.

(iv) To test the importance of the presence of gas, we have simulated binary mergers with mass ratio 2:1 with either 10 or 33 per cent of gas. We do not find major differences in the morphology and the kinematics of the merger remnants. There are some visible differences (e.g. the number of newly formed globular clusters) but they do not impact much the kinematics of the remnants and the comparison with the ATLAS^{3D} sample. Higher gas fractions representative of mergers at high redshifts could have a larger impact, though.

(v) All the major remergers of ETG-like galaxy remnants are either classified as fast rotators or close to the boundary between the slow and fast families. Such remnants present clear rotation patterns and do not hold a KDC: all the KDCs in the progenitors have been destroyed during the remerger and none has been created during the merger event.

(vi) The properties of the fast rotators formed in our simulations are consistent with some observed fast rotators of the ATLAS^{3D} sample. Some of the simulated slow rotators may also be associated with a few observed 2σ galaxies which present clear evidence of an apparent counter-rotating stellar component.

(vii) Our simulations cannot, however, account for the other classes of slow rotators which are intrinsically rounder than any of our major merger remnants: these galaxies are generally massive and have certainly a more complex history. To simulate these galaxies, the full cosmological context of their formation history has to be considered, including major merger(s), repeated minor mergers, stellar mass loss and also smooth accretion of gas from the cosmic filaments.

ACKNOWLEDGMENTS

MBois and TN acknowledge support from the DFG Cluster of Excellence 'Origin and Structure of the Universe'. MC acknowledges support from a Royal Society University Research Fellowship. This work was supported by the rolling grants 'Astrophysics at Oxford' PP/E001114/1 and ST/H002456/1 and visitors grants PPA/V/S/2002/00553, PP/E001564/1 and ST/H504862/1 from the UK Research Councils. RLD acknowledges travel and computer grants from Christ Church, Oxford, and support from the Royal Society in the form of a Wolfson Merit Award 502011.K502/jd. RLD also acknowledges the support of the European Southern Observatory (ESO) Visitor Programme which funded a 3 month stay in 2010. SK acknowledges support from the Royal Society Joint Projects Grant JP0869822. RMcD is supported by the Gemini Observatory, which is operated by the Association of Universities for Research in Astronomy, Inc., on behalf of the international Gemini partnership of Argentina, Australia, Brazil, Canada, Chile, the United Kingdom and the United States of America. MS acknowledges support from an STFC Advanced Fellowship ST/F009186/1. NS and TD acknowledge support from an STFC studentship. The authors acknowledge financial support from ESO.

REFERENCES

Abadi M. G., Navarro J. F., Fardal M., Babul A., Steinmetz M., 2010, MNRAS, 407, 435
Athanassoula E., Bureau M., 1999, ApJ, 522, 699
Bacon R. et al., 2001, MNRAS, 326, 23
Balcells M., González A. C., 1998, ApJ, 505, 109
Balcells M., Quinn P. J., 1990, ApJ, 361, 381
Barnes J. E., 1992, ApJ, 393, 484
Barnes J. E., 2002, MNRAS, 333, 481
Bendo G. J., Barnes J. E., 2000, MNRAS, 316, 315
Bois M. et al., 2010, MNRAS, 406, 2405
Bournaud F., Combes F., Jog C. J., 2004, A&A, 418, 27
Bournaud F., Jog C. J., Combes F., 2005, A&A, 437, 69
Bournaud F., Jog C. J., Combes F., 2007, A&A, 476, 1179
Bournaud F., Duc P.-A., Emsellem E., 2008, MNRAS, 389, L8
Bournaud F., Elmegreen B. G., Teyssier R., Block D. L., Puerari I., 2010, MNRAS, 409, 1088
Bournaud F. et al., 2011, ApJ, 730, 4
Burkert A., 1995, ApJ, 447, L25
Burkert A., 2006, Comptes Rendus Physique, 7, 433
Burkert A., Naab T., Johansson P. H., Jesseit R., 2008, ApJ, 685, 897
Cappellari M., Copin Y., 2003, MNRAS, 342, 345
Cappellari M. et al., 2007, MNRAS, 379, 418
Cappellari M. et al., 2011, MNRAS, 413, 813 (Paper I)
Chilingarian I. V., Di Matteo P., Combes F., Melchior A.-L., Semelin B., 2010, A&A, 518, 61
Coccato L. et al., 2009, MNRAS, 394, 1249
Cox T. J., Dutta S. N., Di Matteo T., Hernquist L., Hopkins P. F., Robertson B., Springel V., 2006a, ApJ, 650, 791
Cox T. J., Jonsson P., Primack J. R., Somerville R. S., 2006b, MNRAS, 373, 1013
Cox T. J., Jonsson P., Somerville R. S., Primack J. R., Dekel A., 2008, MNRAS, 384, 386
Cretton N., Naab T., Rix H.-W., Burkert A., 2001, ApJ, 554, 291
Crocker A. F., Jeong H., Komugi S., Combes F., Bureau M., Young L. M., Yi S., 2009, MNRAS, 393, 1255
Daddi E. et al., 2010, ApJ, 713, 686

Davies R. L. et al., 2001, ApJ, 548, 33
de Zeeuw P. T., Franx M., 1991, ARA&A, 29, 239
de Zeeuw P. T. et al., 2002, MNRAS, 329, 513
Dekel A., Sari R., Ceverino D., 2009, ApJ, 703, 785
Di Matteo P., Combes F., Melchior A.-L., Semelin B., 2007, A&A, 468, 61
Di Matteo P., Bournaud F., Martig M., Combes F., Melchior A.-L., Semelin B., 2008, A&A, 492, 31
Di Matteo P., Jog C. J., Lehnert M. D., Combes F., Semelin B., 2009, A&A, 501, 9
Elmegreen B. G., Scalo J., 2004, ARA&A, 42, 211
Elmegreen B. G., Bournaud F., Elmegreen D. M., 2008, ApJ, 688, 67
Emsellem E. et al., 2007, MNRAS, 379, 401 (E+07)
Emsellem E. et al., 2011, 414, 888 (Paper III)
Fathi K., Beckman J. E., Piñol-Ferrer N., Hernandez O., Martínez-Valpuesta I., Carignan C., 2009, ApJ, 704, 1657
Feldmann R., Mayer L., Carollo C. M., 2008, ApJ, 684, 1062
Franx M., Illingworth G., 1988, ApJ, 327, 55
Franx M., Illingworth G., de Zeeuw P. T., 1991, ApJ, 383, 112
Genel S. et al., 2008, ApJ, 688, 789
Genel S., Bouché N., Naab T., Sternberg A., Genzel R., 2010, ApJ, 719, 229
Governato F. et al., 2009, MNRAS, 398, 312
Graham A., Worley C. C., 2008, MNRAS, 388, 1708
Hernquist L., 1990, ApJ, 356, 359
Hernquist L., Barnes J. E., 1991, Nat, 354, 210
Hoffman L., Cox T. J., Dutta S., Hernquist L., 2010, ApJ, 723, 818
Hopkins P. F., Hernquist L., Cox T. J., Dutta S. N., Rothberg B., 2008, ApJ, 679, 156
Hopkins P. F., Cox T. J., Younger J. D., Hernquist L., 2009, ApJ, 691, 1168
Hopkins P. F. et al., 2010, ApJ, 715, 202
Jedrzejewski R., Schechter P. L., 1988, ApJ, 330, 87
Jesseit R., Naab T., Burkert A., 2005, MNRAS, 360, 1185
Jesseit R., Naab T., Peletier R. F., Burkert A., 2007, MNRAS, 376, 997
Jesseit R., Cappellari M., Naab T., Emsellem E., Burkert A., 2009, MNRAS, 397, 1202
Johansson P. H., Naab T., Burkert A., 2009, ApJ, 690, 802
Kennicutt R. C., Jr, 1998, ApJ, 498, 541
Khochfar S., Burkert A., 2003, ApJ, 597, 117
Khochfar S., Burkert A., 2006, A&A, 445, 403
Khochfar S., Silk J., 2006, MNRAS, 370, 902
Konstantopoulos I. S. et al., 2010, ApJ, 723, 197
Krajnović D. et al., 2008, MNRAS, 390, 93
Krajnović D. et al., 2011, 414, 2923 (Paper II)
McDermid R. M. et al., 2006, MNRAS, 373, 906
Mac Low M.-M., 1999, ApJ, 524, 169
Martig M., Bournaud F., 2008, MNRAS, 385, 38
Martig M., Bournaud F., 2010, ApJ, 714, L275
Martig M., Bournaud F., Teyssier R., Dekel A., 2009, ApJ, 707, 250
Michel-Dansac L. et al., 2010, ApJ, 717, 143
Mihos J. C., Hernquist L., 1994, ApJ, 437, 611
Mihos J. C., Walker I. R., Hernquist L., Mendes de Oliveira C., Bolte M., 1995, ApJ, 447, L87
Moster B. P., Macciò A. V., Somerville R. S., Johansson P. H., Naab T., 2010, MNRAS, 403, 1009
Murphy J. D., Gebhardt K., Adams J. J., 2011, ApJ, 729, 129
Naab T., Burkert A., 2003, ApJ, 597, 893
Naab T., Trujillo I., 2006, MNRAS, 369, 625
Naab T., Jesseit R., Burkert A., 2006a, MNRAS, 372, 839
Naab T., Khochfar S., Burkert A., 2006b, ApJ, 636, 81
Naab T., Johansson P. H., Ostriker J. P., Efstathiou G., 2007, ApJ, 658, 710
Naab T., Johansson P. H., Ostriker J. P., 2009, ApJ, 699, 178
Navarro J. F. et al., 2010, MNRAS, 402, 21
Nieto J.-L., Bender R., Surma P., 1991, A&A, 244, 37
Oser L., Ostriker J. P., Naab T., Johansson P. H., Burkert A., 2010, ApJ, 725, 2312
Powell L. C., Bournaud F., Chapon D., Devriendt J., Slyz A., Teyssier R., 2011, in Alves J., Elmegreen B., Trimble V., eds, Proc. IAU Symp. 270, Computational Star Formation. Cambridge Univ. Press, Cambridge, p. 487
Proctor R. N., Forbes D. A., Romanowsky A. J., Brodie J. P., Strader J., Spolaor M., Mendel J. T., Spitler L., 2009, MNRAS, 398, 91
Qu Y., Di Matteo P., Lehnert M., van Driel W., Jog C. J., 2010, A&A, 515, 11
Renaud F., Boily C. M., Naab T., Theis C., 2009, ApJ, 706, 67
Robertson B., Bullock J. S., Cox T. J., Di Matteo T., Hernquist L., Springel V., Yoshida N., 2006, ApJ, 645, 986
Rothberg B., Joseph R. D., 2006, AJ, 132, 976
Schmidt M., 1959, ApJ, 129, 243
Scorza C., Bender R., 1995, A&A, 293, 20
Springel V., 2000, MNRAS, 312, 859
Springel V., 2005, MNRAS, 364, 1105
Springel V., Hernquist L., 2005, ApJ, 622, 9
Springel V. Di Matteo T., Hernquist L., 2005, ApJ, 620, L79
Tacconi L. J. et al., 2010, Nat, 463, 781
Teyssier R., Chapon D., Bournaud F., 2010, ApJ, 720, 149
Thomas J., Jesseit R., Naab T., Saglia R. P., Burkert A., Bender R., 2007, MNRAS, 381, 1672
Toomre A., Toomre J., 1972, ApJ, 178, 623
Toth G., Ostriker J. P., 1992, ApJ, 389, 5
Tremblay B., Merritt D., 1996, AJ, 111, 2243
van den Bosch R. C. E., van de Ven G., Verolme E. K., Cappellari M., de Zeeuw P. T., 2008, MNRAS, 385, 647
Weijmans A.-M. et al., 2009, MNRAS, 398, 561
Weil M. L., Hernquist L., 1994, ApJ, 431, 79
Weil M. L., Hernquist L., 1996, ApJ, 460, 101
Wuyts S., Cox T. J., Hayward C. C., Franx M., Hernquist L., Hopkins P. F., Jonsson P., van Dokkum P. G., 2010, ApJ, 722, 1666

APPENDIX A: PROJECTED VELOCITY MAPS OF BINARY MERGERS AND REMERGERS

All simulations used for this study are listed here. For each simulation, an edge-on view of the velocity field (with the iso-magnitude contours in black) and its associated λ_R profile are plotted.

The binary merger simulations are classified in this way.

(i) A figure corresponds to mergers with the same mass ratio, e.g. Fig. A1 shows the binary mergers of mass ratio 1:1.

(ii) A group of six projections associated with their λ_R profiles correspond to a specific orbit of merging (*dd*, *rd* or *rr* orbits).

(iii) The six projections correspond to the different initial conditions for a specific orbit of merging (*0*, *im*, *ip*, *Rm*, *Vm*, *Vp*; see Table 2).

(iv) The label of the simulation (e.g. m31ddip) and the velocity cut are noted in the projected velocity maps.

The remergers are classified in this way.

(i) A figure corresponds to remergers of two remnants of binary mergers with the same initial mass ratio; e.g. Fig. A6 shows the remergers of two remnants of binary mergers of mass ratio 1:1.

(ii) The four subpanels of a figure correspond to the four different orbit of merging (*dd*, *dr*, *rd* or *rr*).

(iii) The label of the simulation (e.g. rem21g10+Sdd) and the velocity cut are noted in the projected velocity maps.

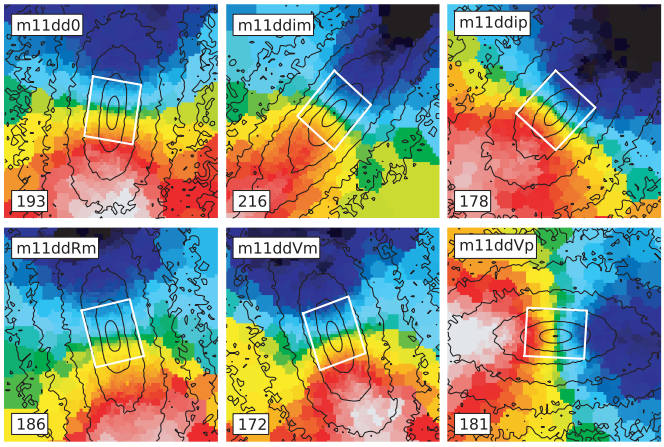

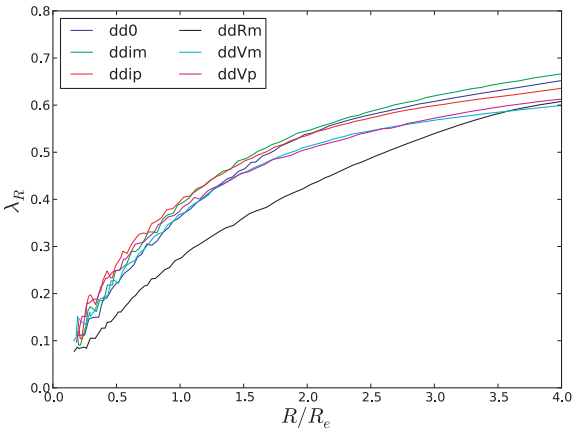

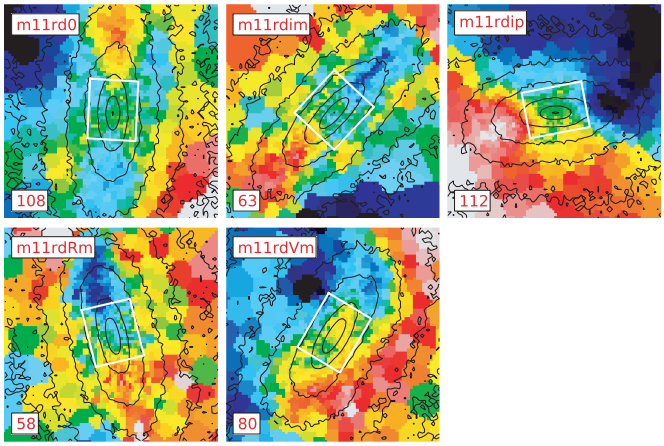

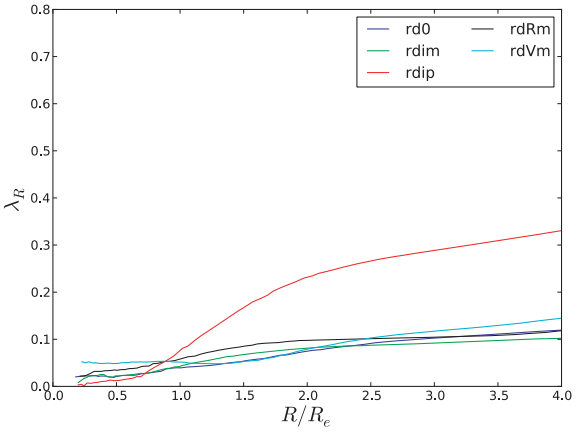

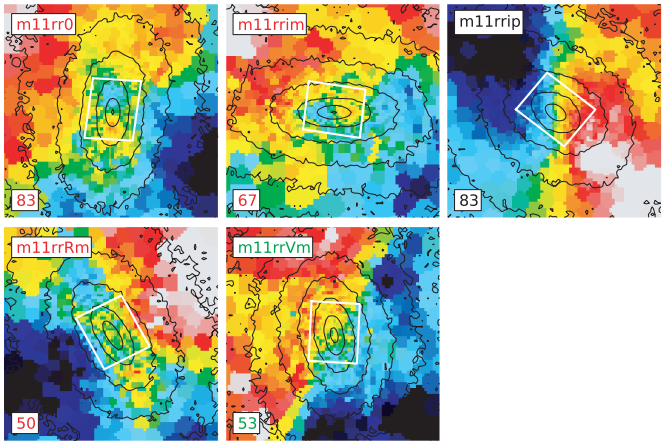

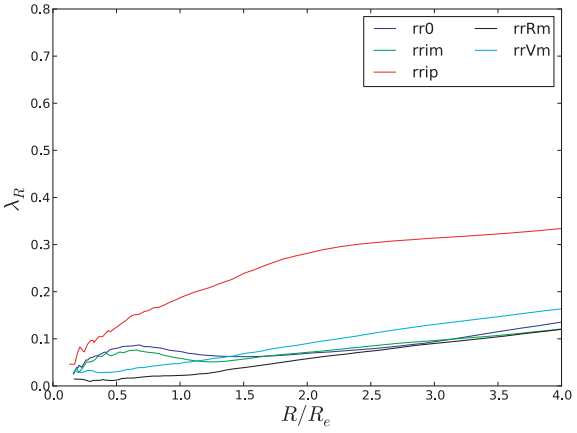

Figure A1. Left: edge-on projection of the velocity field for the binary mergers of mass ratio 1:1 for the three types of orbits (top: *dd* orbit; middle: *rd* orbit; bottom: *rr* orbit). The black lines correspond to the iso-magnitude contours. The different initial conditions and velocity cuts are noted in the subpanels: the colour of the text indicates if the galaxy is classified as a fast rotator (black), a slow rotator with a KDC (red) or a slow rotator without KDC (green); the KDC may not be visible under the edge-on projection but is visible for most of the others. The field of view is $15 \times 15\,\mathrm{kpc}^2$. The white rectangle indicates a typical field covered by the instrument SAURON and corresponds to a field of $41 \times 33\,\mathrm{arcsec}^2$ for a galaxy at a distance of 20 Mpc; its orientation follows the photometric position angle taken at $3R_\mathrm{e}$. Right: the corresponding λ_R profiles as a function of the radius R divided by the effective radius R_e of the edge-on projection.

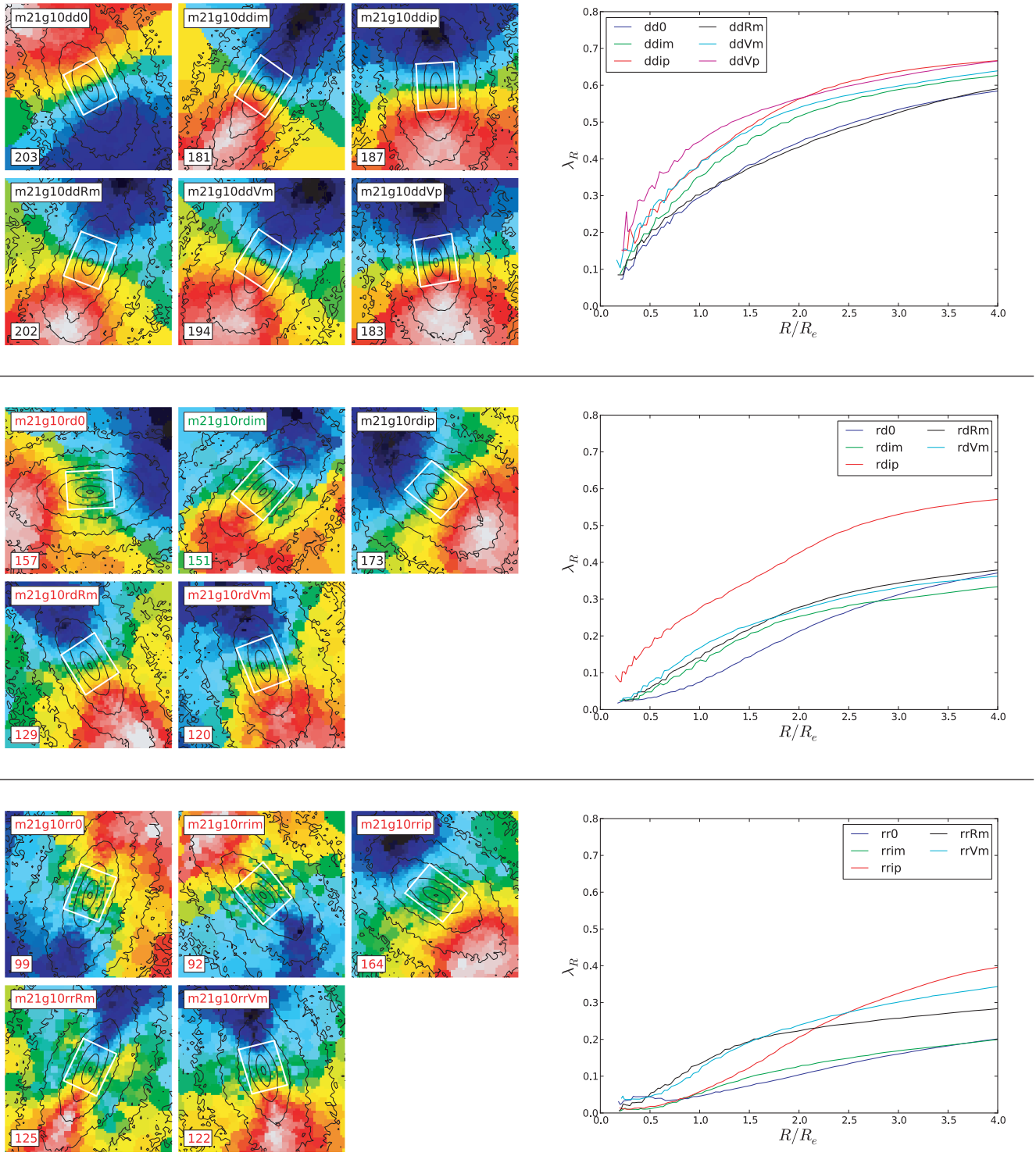

Figure A2. Same as Fig. A1 for the binary mergers of mass ratio 2:1 with 10 per cent of gas.

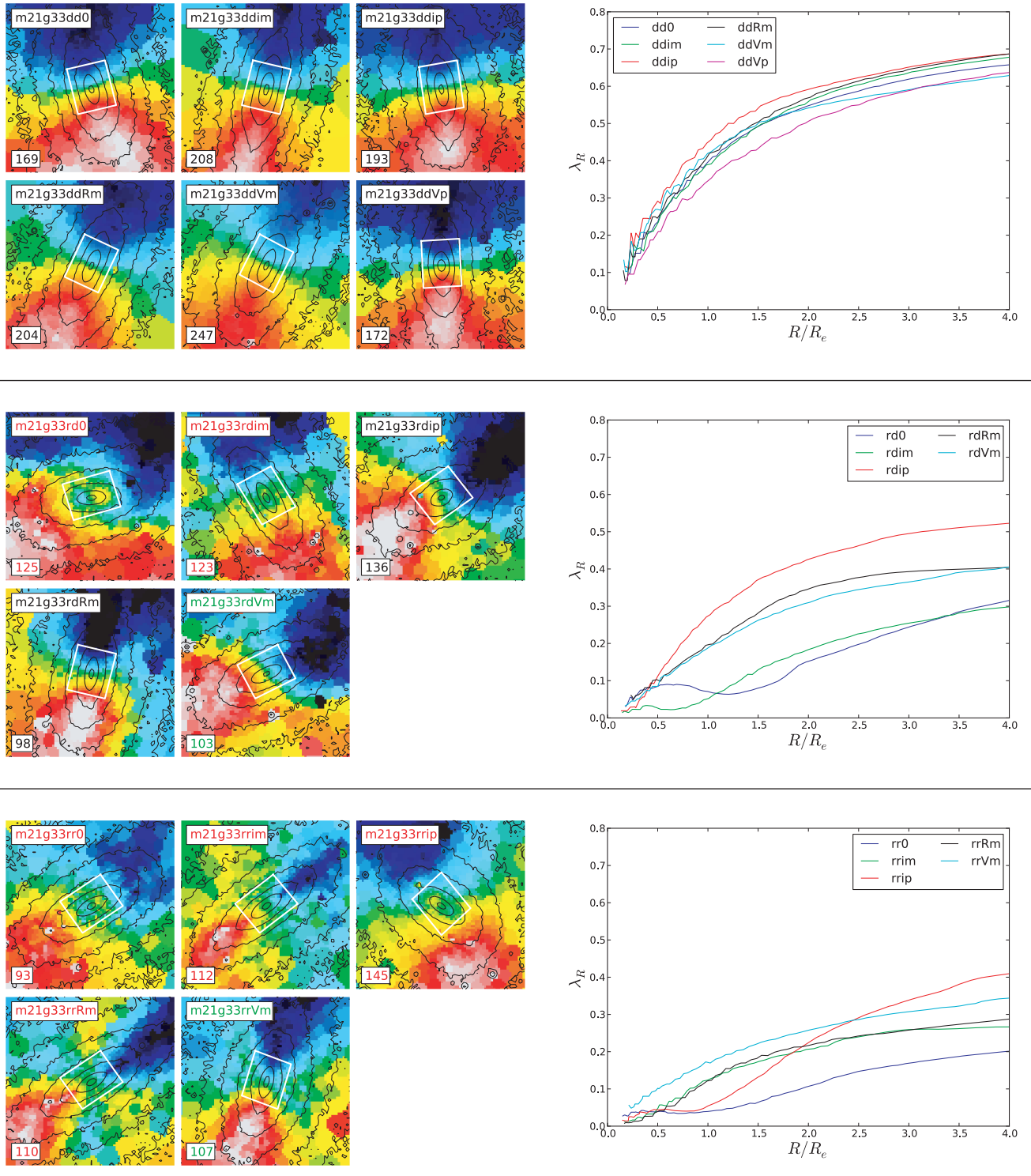

Figure A3. Same as Fig. A1 for the binary mergers of mass ratio 2:1 with 33 per cent of gas.

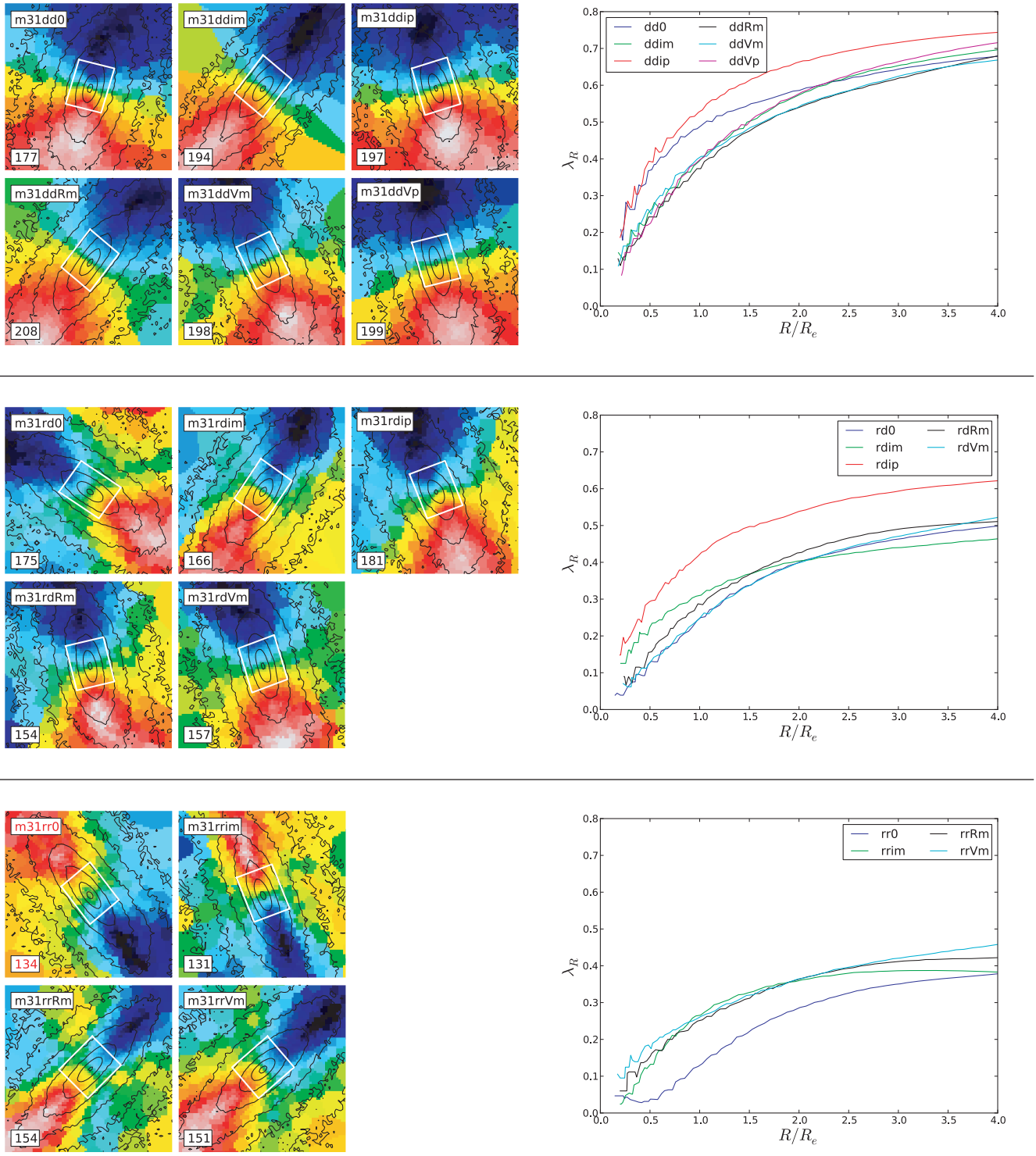

Figure A4. Same as Fig. A1 for the binary mergers of mass ratio 3:1.

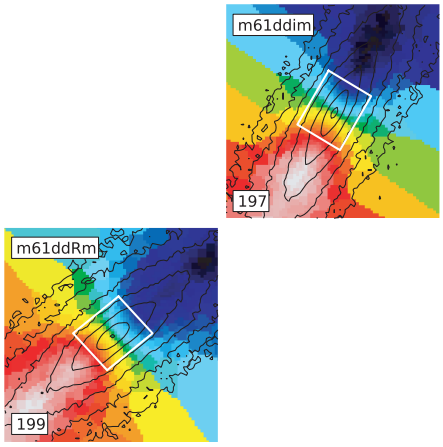

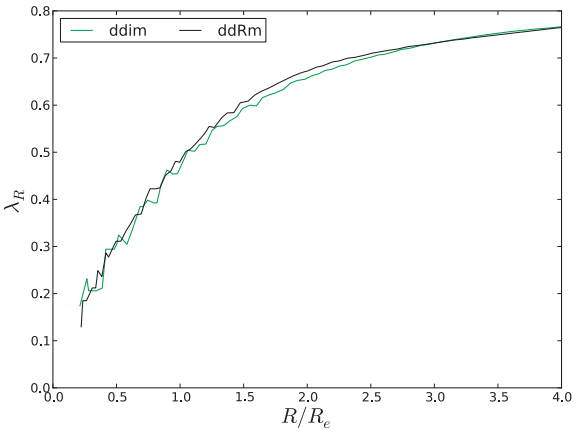

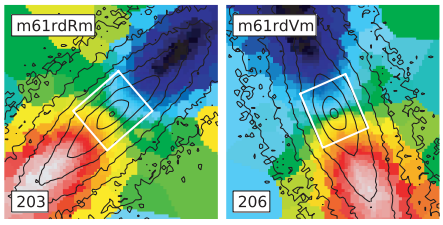

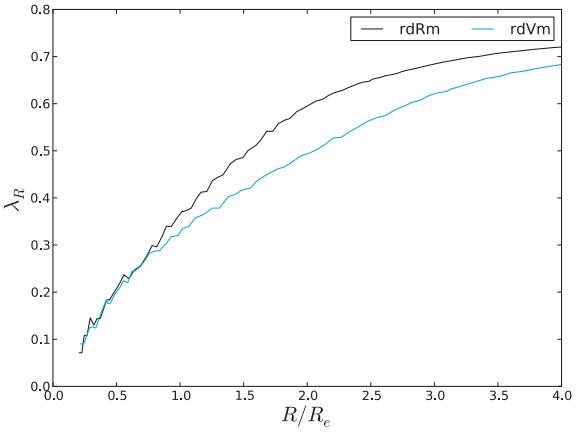

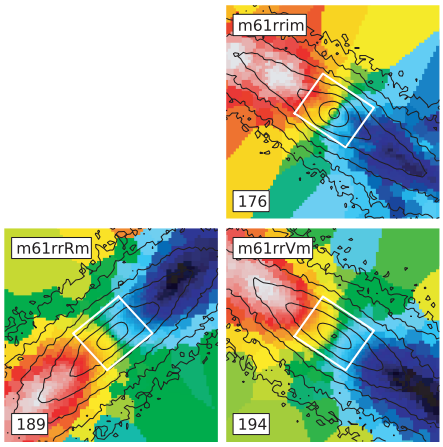

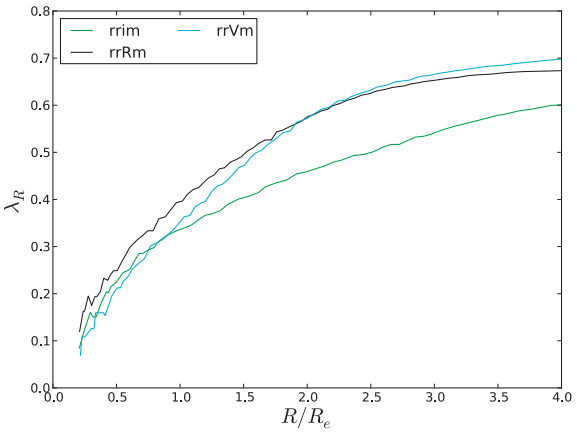

Figure A5. Same as Fig. A1 for the binary mergers of mass ratio 6:1.

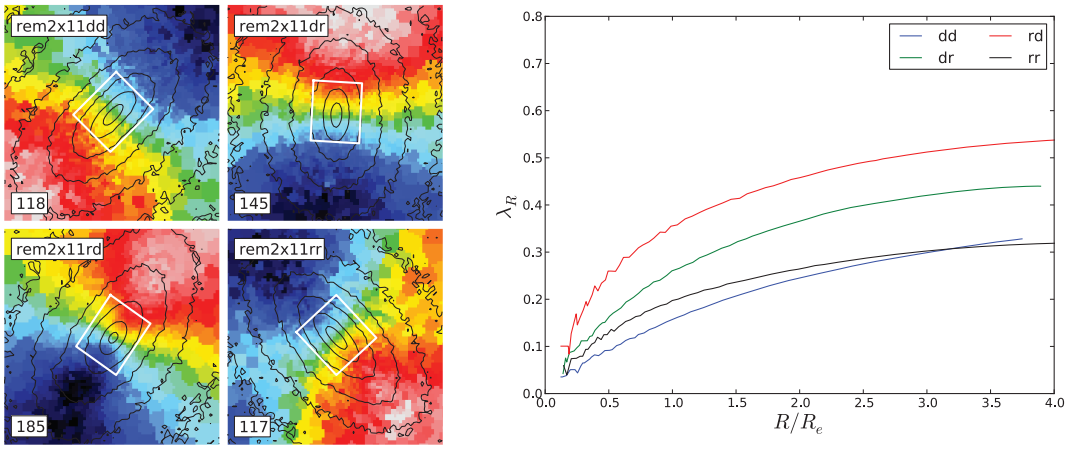

Figure A6. Left: edge-on projection of the velocity field for remergers of two remnants of binary mergers of mass ratio 1:1. The black lines correspond to the iso-magnitude contours. The different initial angular momentum spins and velocity cuts are noted in the subpanels. The field of view is 15 × 15 kpc^2. The white rectangle indicates a typical field covered by the instrument SAURON and corresponds to a field of 41 × 33 arcsec^2 for a galaxy at a distance of 20 Mpc; its orientation follows the photometric position angle taken at $3R_e$. Right: the corresponding λ_R profiles as a function of the radius R divided by the effective radius R_e of the edge-on projection.

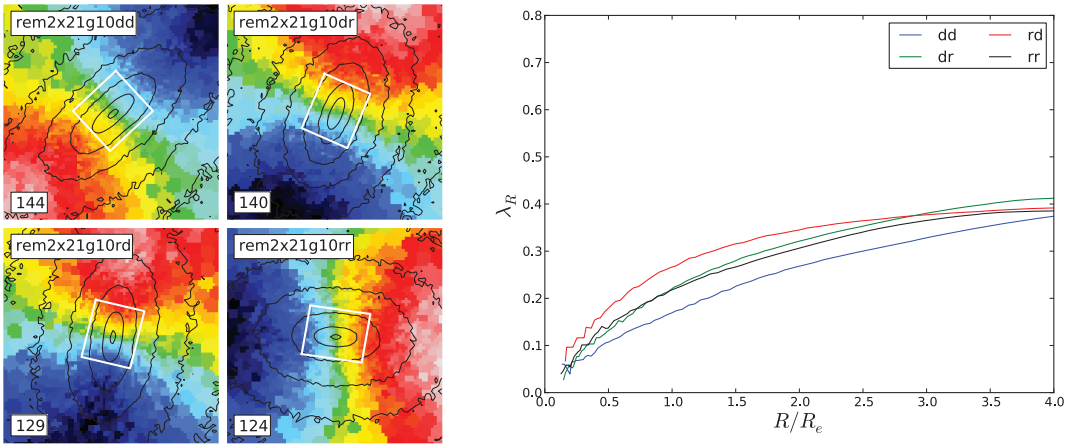

Figure A7. Same as Fig. A6 for remergers of two remnants of binary mergers of mass ratio 2:1 with 10 per cent of gas.

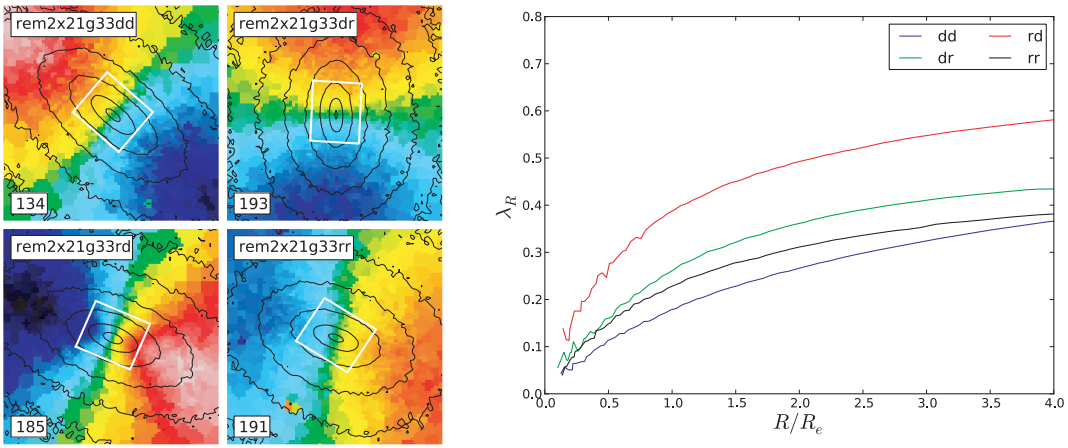

Figure A8. Same as Fig. A6 for remergers of two remnants of binary mergers of mass ratio 2:1 with 33 per cent of gas.

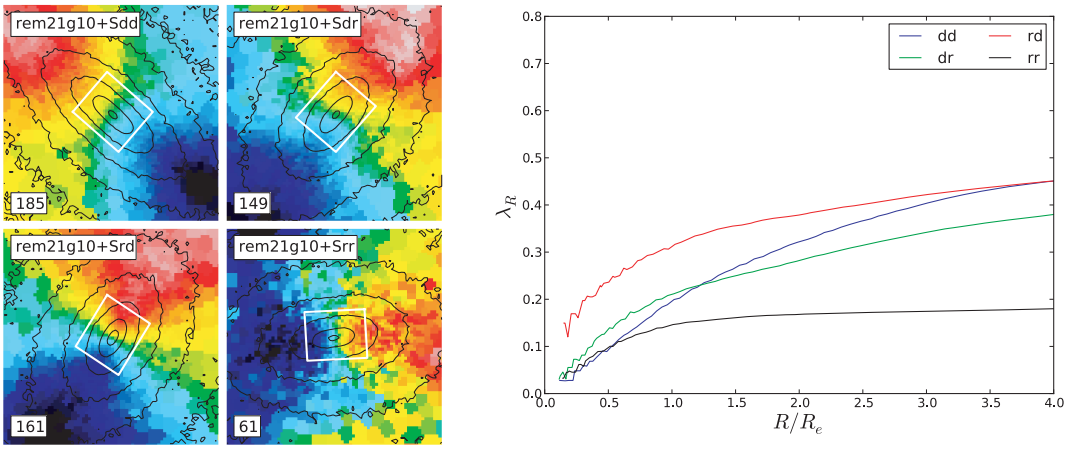

Figure A9. Same as Fig. A6 for remergers between a remnant of binary mergers of mass ratio 2:1 with 10 per cent of gas and a spiral galaxy.

This paper has been typeset from a TEX/LATEX file prepared by the author.